1521-009X/49/4/330–336$35.00
DRUG METABOLISM AND DISPOSITION

https://doi.org/10.1124/dmd.120.000337
Drug Metab Dispos 49:330–336, April 2021

Evaluation of Tissue Binding in Three Tissues across Five Species and Prediction of Volume of Distribution from Plasma Protein and Tissue Binding with an Existing Model[S]

Frederick Hsu, Yi-Chen Chen, and Fabio Broccatelli

Drug Metabolism and Pharmacokinetics, Genentech, Inc., South San Francisco, California

Received December 17, 2020; accepted January 25, 2021

ABSTRACT

Volume of distribution (V_d) is a primary pharmacokinetic parameter used to calculate the half-life and plasma concentration-time profile of drugs. Numerous models have been relatively successful in predicting V_d, but the model developed by Korzekwa and Nagar is of particular interest because it utilizes plasma protein binding and microsomal binding data, both of which are readily available in vitro parameters. Here, Korzekwa and Nagar's model was validated and expanded upon using external and internal data sets. Tissue binding, plasma protein binding, V_d, physiochemical, and physiologic data sets were procured from literature and Genentech's internal data base. First, we investigated the hypothesis that tissue binding is primarily governed by passive processes that depend on the lipid composition of the tissue type. The fraction unbound in tissues (fu_{tissue}) was very similar across human, rat, and mouse. In addition, we showed that dilution factors could be generated from nonlinear regression so that one fu_{tissue} value could be used to estimate another one regardless of species. More importantly, results suggested that microsomes could serve as a surrogate for tissue binding. We applied the parameters from Korzekwa and Nagar's V_d model to two distinct liver microsomal data sets and found remarkably close statistical results. Brain and lung data sets also accurately predicted V_d, further validating the model. V_d prediction accuracy for compounds with log $D_{7.4} > 1$ significantly outperformed that of more hydrophilic compounds. Finally, human V_d predictions from Korzekwa and Nagar's model appear to be as accurate as rat allometry and slightly less accurate than dog and cynomolgus allometry.

SIGNIFICANCE STATEMENT

This study shows that tissue binding is comparable across five species and can be interconverted with a dilution factor. In addition, we applied internal and external data sets to the volume of distribution model developed by Korzekwa and Nagar and found comparable V_d prediction accuracy between the V_d model and single-species allometry. These findings could potentially accelerate the drug research and development process by reducing the amount of resources associated with in vitro binding and animal experiments.

Introduction

Volume of distribution (V_d) is a proportionality constant between the observed concentration and the amount of drug in the body. This is used in compartmental pharmacokinetic (PK) modeling to describe the plasma concentration-time profile of drugs. Although V_d is an important parameter for data description, its biologic relevance is not emphasized in classic compartmental modeling and PK theory. Several authors (Oie and Tozer, 1979; Rodgers and Rowland, 2007; Poulin and Theil 2009) addressed the physiologic relevance of the V_d term by using mechanistic modeling approaches; the aim of these studies was to describe V_d in physiologically relevant terms involving distribution in blood and tissues. Oie and Tozer originally described the tissue binding component by lumping binding to all tissues into a single term (V_t). More recent physiologically based tissue partitioning models aim to predict distribution in each major organ to better capture the shape of the PK profile. In these models, different tissues are characterized based on their composition; therefore, binding may vary considerably across tissues depending on the characteristics of the drug. For example, in tissue partitioning models, the distribution of a given compound in the adipose tissue might be predicted as substantially different from its distribution in muscles because of the heterogenous characteristic of the tissues.

Berellini and Lombardo (2019) used Oie and Tozer's model as a base to estimate V_t for a large set of marketed drugs by employing simple calculated physicochemical parameters in a data-driven linear model. This approach delivered a fully reproducible and accurate model that remains one of the better-validated approaches in literature given the size of the data set employed. Because this model is based on calculated parameters such as pK_a and lipophilicity, the effect of miscalculations for these input parameters is a considerable unknown.

Recently, Ryu et al. (2020) published a data set of 80 compounds tested in binding experiments across different tissues and species. This study highlighted the idea that binding to tissues is comparable across

This work received no external funding.
https://doi.org/10.1124/dmd.120.000337.
[S]This article has supplemental material available at dmd.aspetjournals.org.

ABBREVIATIONS: AAFE, absolute average fold error; AAG, α-acid glycoprotein; AFE, average fold error; AUC, area under the curve; CL, clearance; cyno, cynomolgus; D, dilution factor; fu_{brain}, fraction unbound in brain; fu_{mic}, fraction unbound in microsome; fu_p, fraction unbound in plasma; fu_{tissue}, fraction unbound in tissue; LK_L, lipid concentration L times the lipid binding constant K_L; NCA, noncompartmental analysis; PK, pharmacokinetic; R_1, the ratio of the concentration of plasma proteins in the tissue to the concentration of plasma proteins in the plasma; V_d, volume of distribution; V_p, plasma volume; V_t, tissue volume.

species and organs, in agreement with previously published work (Barr et al., 2019). Indirectly, these findings recapitulate the findings presented by Lombardo et al., which showed that although species allometry is a good predictor of V_d, it has limited accuracy in clearance (CL) prediction. Unlike metabolism, which is primarily determined by enzymatic processes that differ across species, distribution is primarily dominated by passive processes that depend on tissue composition and perfusion.

Although the work of Ryu et al. (2020) supports tissue binding predictions from a single tissue measurement, it does not attempt to further translate these findings into V_d predictions. Currently, at Genentech, the only tissue binding measurements routinely available during early discovery stages are performed on microsomes. The main use of microsomal binding data is to predict the in vitro CL of a free drug. Microsomes are artificial constructs of unsorted nature; however, they maintain all the major lipid components that are believed to be relevant for tissue binding.

Recently, Korzekwa and Nagar (2017) developed a model sharing commonalities with the Oie-Tozer approach, which described distribution into tissues by using a lumped V_t term, estimated based on microsomal binding; compared with the pioneering work presented by Rodgers and Rowland (2007), this model is sensitive to changes in plasma protein binding for strong bases and relies on a direct measurement to a biologic tissue rather than an estimate based on physicochemical parameters. This work is based on a small data set derived from human PK experiments only. In this work, we attempt to generalize observations published by Ryu et al. (2020) and by Korzekwa and Nagar (2017) to produce a distribution model readily available during the early stages of research that can be applied across different species. In addition, we seek to define the applicability domain of the resulting model with respect to lipophilicity, charge, and accuracy in preclinical species. Beyond increased accuracy, this methodology promises significant logistic advantages because of the reliance on a low number of in vitro measurements (microsomal binding and plasma protein binding) that are also necessary when predicting in vivo CL of metabolically eliminated compounds. These findings could support the optimization of drug half-life using in vitro (as opposed to in vivo) experiments.

Materials and Methods

Tissue and Plasma Protein Binding Data. Data sets incorporating fraction unbound in tissue (fu_{tissue}) measurements for brain, lung, and microsomes across three different species (human, mouse, and rat) were obtained from Genentech's internal small molecules data base; this search did not include macrocyclic compounds, therapeutic peptides, or bivalent inhibitors. When multiple values were available, the geometric mean was adopted. Rapid equilibrium dialysis was used to determine fu_{tissue} as previously described (Leung et al., 2020); we performed tissue binding experiments with a 4-hour incubation time, and tissue homogenates were obtained from BioIVT (https://bioivt.com/).

Calculated fu_{mic} values were derived using Genentech's internal machine learning model and reported in the Supplemental Material (Supplemental Table 3). Only prospective predictions (predictions run before having experimental measurements) were incorporated to avoid biasing the performance as a result of training set fitting. Since the model was only introduced 1.5 years ago, the prospective predictions are available for 160 compounds.

All the available fu_{tissue} values greater than 0.001 were included in the data set; highly bound compounds were excluded because of the experimental uncertainty typically associated with rapid equilibrium dialysis approaches (Chen et al., 2019; Leung et al., 2020).

Values for fraction unbound in plasma (fu_p) greater than 0.001 and obtained in experiments for which the incubation time was 24 hours were included in the data set. Compounds that were highly bound in the same assay (>99.9%) were excluded because of the lower confidence associated with the experiment (Waters et al., 2008; Chen et al., 2019). Plasma protein binding experiments that were run with a 6-hour incubation were included in additional validation sets (brain and lung binding data sets); because of the shorter incubation time, the adopted inclusion criteria were modified to fu_p values greater than 0.1.

Volume of Distribution Data. V_d estimates from noncompartmental analysis (NCA) were performed using Phoenix WinNonlin version 6.4 (Certara USA, Inc., Princeton, NJ). NCA requires that the plasma concentration-time profile adequately captures the area under the curve (AUC); experiments for which a substantial fraction of the AUC is extrapolated may result in less accurate quantifications of the primary PK parameters. To address this limitation, a cutoff of 20% of extrapolated AUC was applied as an inclusion criterion for experiments to be incorporated in our data set. The estimated V_d may differ based on the reference biologic matrix used in the NCA analysis (blood vs. plasma). This is particularly true when blood-to-plasma partition tends to be high for a given chemical scaffold. Historically, information about the reference biologic matrix used in the NCA PK analysis has not always been made available in our corporate data base. We therefore excluded scaffolds for which blood-to-plasma partitioning typically exceeded a value of two and for which the biologic matrix used for the analysis is not known (2 projects out of 29). Only parameters derived from intravenous experiments in mouse, rat, dog, cynomolgus, and human were included in the data set. Three data sets (brain, lung, and microsome) were used to predict V_d (Supplemental Tables 1 and 2). Brain and lung data sets included four species (cyno, dog, rat, mouse), and the microsome data set included five species (human, cyno, dog, rat, mouse). Intravenous human V_d data were collected from Berellini et al. (Lombardo et al., 2018) or, when not available, from the DrugBank data base (https://www.drugbank.ca/).

Physiologic Parameters. Plasma volume (V_p) and tissue volume (V_t) parameters for each species were obtained from literature and are shown in Table 1 (Davies and Morris, 1993). Cynomolgus physiologic values were assumed to be same as rhesus. V_p is calculated by dividing the plasma volume (liters) by the typical body weight of the species, whereas V_t is calculated by subtracting total body water (liters) by the blood volume (liters) and dividing that difference by the typical body weight of the species. Total body water volume is a sum of intracellular and extracellular fluid, and blood was not considered to be a tissue. Thus, any volume of liquid that was not blood was assumed to be tissue volume. R_1, as described by Korzekwa and Nagar, is the ratio of the concentration of plasma proteins in the tissue to the concentration of plasma proteins in the plasma. For neutral and acidic compounds, R_1 was calculated to be 0.116 in humans (60% extraplasma albumin in V_t divided by 40% plasma albumin in V_p). Assumptions for the R_1 values to be used for zwitterionic species are not explicitly mentioned in Korzekwa and Nagar's paper; however, in the current work, an R_1 value of 0.116 was used under the assumption that zwitterionic compounds will predominantly bind to plasma albumin. For basic compounds, R_1 was calculated to be 0.052, as they are expected to predominantly bind to α-acid glycoprotein (AAG) (40% AAG in V_t divided by 60% plasma AAG in V_p). Although R_1 might differ slightly from species to species, we observed that small changes in R_1 values have minimal impact on the results of the model. Thus, an R_1 value of either 0.116 or 0.052 was adopted for all species.

Experimental and Calculated Physicochemical Properties. In the work published by Korzekwa and Nagar, information about the ionization class is used to determine the value of R_1. To that end, calculated pK_a values were obtained using Moka (https://www.moldiscovery.com/software/moka/). Compounds were classified as basic, acidic, zwitterionic, or neutral based on the calculated charge at pH 7.4. Compounds for which the pK_a value was within 0.5 units from the cutoff of pH 7.4 were excluded because of the possible ambiguity in the assignment of

TABLE 1

Physiologic parameters for human, cyno, dog, rat, and mouse

Species	V_p	V_t	R_1 (Acid, Neutral, Zwitterion)	R_1 (Base)
	l/kg	*l/kg*		
Human	0.043	0.557	0.116	0.052
Cyno	0.0448	0.6196	0.116	0.052
Dog	0.0515	0.5136	0.116	0.052
Rat	0.0332	0.614	0.116	0.052
Mouse	0.05	0.64	0.116	0.052

ionic species resulting from potential errors in the calculated pK_a value. Notably, the difference in R_1 values for different classes is relatively small; additionally, the R_1 term becomes important for only a subclass of compounds (highly bound with low affinity to tissues). From a practical standpoint, assumptions on charge will most likely be important for anionic and zwitterionic compounds (typically highly bound to albumin) and unimportant for the other classes. Log $D_{7.4}$ was used as a classification cutoff, and compounds without experimentally measured log $D_{7.4}$ were excluded from Genentech's internal preclinical data sets. The lipophilicity assay is performed for most compounds synthesized at Genentech; therefore, this further selection criterion had a minimal impact on the size of the data set. For marketed drugs, log $D_{7.4}$ values were collected from literature (Benet et al., 2011). When experimental log $D_{7.4}$ was not available in the marketed drugs data set (Supplemental Table 1), this value was calculated using Genentech's internal Quantitative Structure-Activity Relationship model.

Tissue Binding Comparison and Prediction Analysis. Using 236 unique Genentech compounds, 354 binding measurements in total in either microsomes, brain, or lung tissue were compared across human, mouse, and rat. There were more fraction unbound values relative to the number of compounds because binding data were available in multiple species and tissues for certain compounds. In addition, under the assumption that different tissue matrices differ in lipid concentration but the affinity of a compound for lipids does not vary, dilution formulas (eq. 1) were used to estimate binding across different tissues for 352 unique Genentech compounds, yielding 399 predicted binding values. Again, there were more fu_{tissue} values relative to the number of compounds because of the availability of binding data in multiple tissues for certain compounds.

$$fu_{tissue,2} = \frac{\frac{1}{D}}{\left(\frac{1}{fu_{tissue,1}} - 1\right) + \frac{1}{D}} \tag{1}$$

Dilution factors (D) were derived from nonlinear regression fitting of eq. 1 using the nonlinear least squares function (Rstudio). Once D was obtained, it was used in conjunction with $fu_{tissue,1}$ to predict $fu_{tissue,2}$.

V_d Prediction Analysis. For V_d prediction, Korzekwa and Nagar's linear LK_L model (eq. 2) was used because of the simplicity of the model. The other more complicated models proposed by Korzekwa and Nagar required more inputs but did not significantly improve V_d predictions (Korzekwa and Nagar, 2017). Thus, the authors concluded that the linear LK_L model was the most appropriate model for V_d predictions. To allow direct comparison with the fitted parameters, fu_{mic} measurements at 0.5 mg/ml were converted to 1 mg/ml using eq. 1. Microsome, brain, and lung data sets included a total of 337, 105, and 14 compounds, respectively. For the brain and lung data sets, brain and lung fu were converted to microsomal fu utilizing the previously derived dilution factors. Finally, the nonlinear least squares function was used to fit eq. 2 to obtain coefficients a and b (Rstudio). V_d was then subsequently predicted with the fitted a and b values and the other parameters in eq. 2.

$$V_d = V_p + V_t R_1 (1 - f_{up}) + V_t f_{up} + f_{up}\left(a\left(\frac{1 - f_{umic}}{f_{umic}}\right) + b\right) \tag{2}$$

Statistical Analysis. Statistical analysis included S.E. for the a and b coefficients derived by nonlinear fitting, R^2, AFE (eq. 3), AAFE (eq. 4), percentage within 2-fold error, and percentage within 3-fold error.

$$\text{AFE} = 10^{average\left(log10\left(\frac{Observed}{Predicted}\right)\right)} \tag{3}$$

$$AAFE = 10^{average\left(\left|log10\left(\frac{Observed}{Predicted}\right)\right|\right)} \tag{4}$$

R: Pearson correlations were calculated based on the log of the predicted and observed values for V_d and binding association constant K_{fu}:

$$K_{fu} = \frac{1 - fu}{fu}. \tag{5}$$

Applicability Domain and Comparison with Allometry. The applicability domain of the model was analyzed with respect to lipophilicity and preclinical allometry data. Based on the analysis presented by Benet et al., (2011), a log $D_{7.4}$ value of 1 can be used as a classification cutoff for compounds' route of elimination; that is, compounds with a log $D_{7.4}$ value > 1 are likely to be eliminated via the hepatic metabolic route. By extension, according to the biopharmaceutics drug distribution classification system, the distribution of compounds in this class is less likely to be affected by active transport. This is consistent with the assumptions of the distribution model introduced by Korzekwa and Nagar, which can therefore be expected to show higher V_d prediction accuracy in the high lipophilicity class. According to the same assumptions, the model can be expected to show higher accuracy in higher species (dog and cynomolgus) when a good predictivity is observed in rodents.

Lombardo et al. (2013) assessed the accuracy of allometry methodologies to predict human V_d. For compounds in our data set for which clinical and preclinical data were reported by Lombardo et al. (2013), single-species allometry proportionality scaling methodologies were used to predict human volume of distribution. This data set was collected for the purpose of evaluating an in vitro–only methodology to predict human V_d compared with in vivo methodology. Finally, the accuracy of the model with respect to the ionization class was also investigated.

Results

Tissue Binding. Pfizer scientists have previously demonstrated that binding in different tissues can be extrapolated by applying simple dilution formulas (Ryu et al., 2020). Although this study was rich in the number of tissues analyzed and included measurements across five species, it was limited in the size of the chemical space explored (80 unique compounds). The tissues included in the analysis (adipose, brain, heart, kidney, liver, lung, and muscle) did not include microsomal binding data, which is routinely measured in discovery phases to improve in vitro to in vivo correlations of clearance (Yang et al., 2007). The work presented by Ryu et al. (2020) highlights how tissue binding is driven mostly by nonspecific binding to lipids, which are the primary components of microsomes. Thus, microsomes could serve as a surrogate for binding in other tissues. In our experience, microsomes are the most frequently used biologic matrix for tissue binding measurements in drug discovery, followed by homogenized brain tissues.

By extending the analysis to all the internal Genentech compounds for which binding measurements were available in either microsomes (64), brain (110), or lung (180) tissues, we were able to evaluate the variability of these 354 measurements across different species. Consistent with the findings from Pfizer and Amgen scientists, we found that tissue binding measurements are consistent across different species (Fig. 1). The high correlation value (R^2) and low absolute average fold deviation are within the range of variability expected for experimental replicates within the same experimental conditions for a given compound. About 93% of compounds in Fig. 1 have fu_{tissue} within 2-fold error in the same tissue for different species. Notably, a majority of the outliers (24) are either highly bound compounds ($0.05 < fu < 0.01$), for which experimental determinations are less quantitative, or measurements obtained in lung tissue, for which higher variability is typically observed because of challenges with homogenizing lung tissue (Liang et al., 2011).

Figure 2 shows the 399 predicted versus experimental fu_{tissue} values for 352 Genentech compounds. Nonlinear fitting analysis was employed to determine the dilution factor that can be used to predict binding in a given tissue (e.g., brain) by leveraging measurements for the same compound in different tissues (e.g., microsomes). Dilution factors predicting fu_{mic} from fu_{brain}, fu_{mic} from fu_{lung}, and fu_{lung} from fu_{brain} were 0.0137, 0.007, and 0.59, respectively, and dilution factors predicting fu_{brain} from fu_{mic}, fu_{lung} from fu_{mic}, and fu_{brain} from fu_{lung} were 66.6, 107.8, and 1.67, respectively (Fig. 2). The analysis yielded an R^2 for the affinity term K_{fu} of 0.76 in Fig. 2A and 0.72 in Fig. 2B. Interestingly, because of the asymmetric nature of the relationship between binding affinity (K_{fu}) and the corresponding fraction unbound, the error in the quantitative prediction of fu_{tissue} observed when extrapolating from a matrix with higher lipid content (e.g., brain) to a matrix with lower lipid content (e.g., microsome) is lower compared

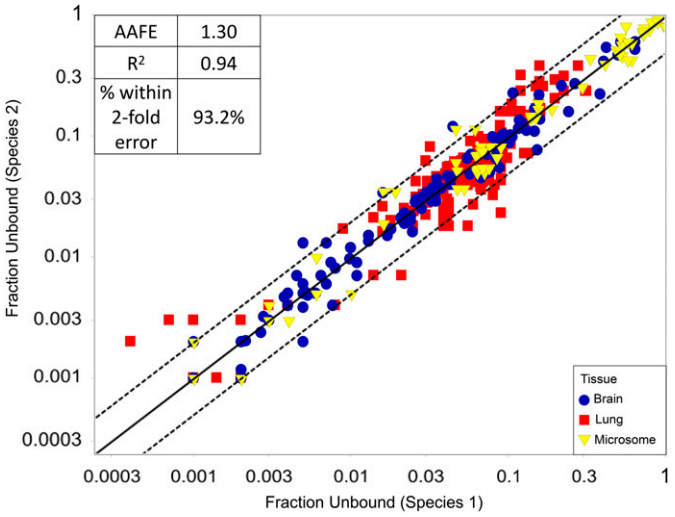

Fig. 1. Comparison of fraction unbound in tissue in three tissues across human, rat, and mouse. Species information is removed from the plot to support the hypothesis that tissue binding is comparable in a given tissue regardless of species. $N = 354$ binding measurements. A table showing AAFE, R^2, and percentage within 2-fold error is located in the top left-hand corner of the figure. The *y*-axis and *x*-axis are presented in log scale. Solid and dotted lines represent best-fit line and 2-fold error, respectively.

with the opposite case. That is, 96% of fu_{tissue} measurements could be predicted from a different tissue with higher lipid content (dilution <1) within 2-fold error, whereas 76% of measurements were within 2-fold error when fu_{tissue} was predicted from a different tissue with a lower lipid content (dilution >1). When the D value is less than 1, fu_{tissue} predictions yield AAFE of 1.19; AAFE increases to 1.66 when the dilution value exceeds 1. These observations can be readily rationalized by looking at a theoretical example. Let us assume a measured fu value of 0.4 in the diluted incubation and a corresponding prediction of 0.8, resulting in a 2-fold deviation between the measured and the predicted fu. Let us now assume a value of D = 20: the extrapolated measured fu for the undiluted incubation is 0.032, whereas the extrapolated predicted fu for the undiluted incubation is 0.17, resulting in a 5.6-fold deviation in fu. This can be generalized by rearranging (1) as follows:

$$y = \frac{\left(1 - f + \frac{1}{D}f\right)x}{1 - fx + \frac{1}{D}fx},$$

in which *y* is the deviation between the predicted and the measured fu in the undiluted incubation, *x* is the deviation between the predicted and the measured fu in the diluted incubation, and *f* is the experimentally measured fu in the diluted incubation. Taken together, these analyses highlight that a single in vitro model can be used to fit in vivo tissue binding from in vitro measurements (either microsomes, lung, or brain binding), which in turn can be supplemented with plasma protein binding data to predict volume of distribution according to eq. 2, as previously proposed by Korzekwa and Nagar.

V_d Prediction with the Korzekwa and Nagar Model. To validate the linear LK_L model introduced by Korzekwa and Nagar, we used the combined external (Supplemental Table 1) and internal data set (Supplemental Table 2) to compare the accuracy of V_d prediction using Korzekwa and Nagar's coefficients with the accuracy of V_d prediction using Genentech's coefficients (Table 2). The coefficients a and b from the two methods exhibited remarkably similar values (Genentech, a = 18.22 and b = 1.76; Korzekwa and Nagar, a = 20 and b = 0.76). With Genentech's fit, 65.0% of the 337 analyzed compounds had predicted V_d values within 2-fold of observed V_d,

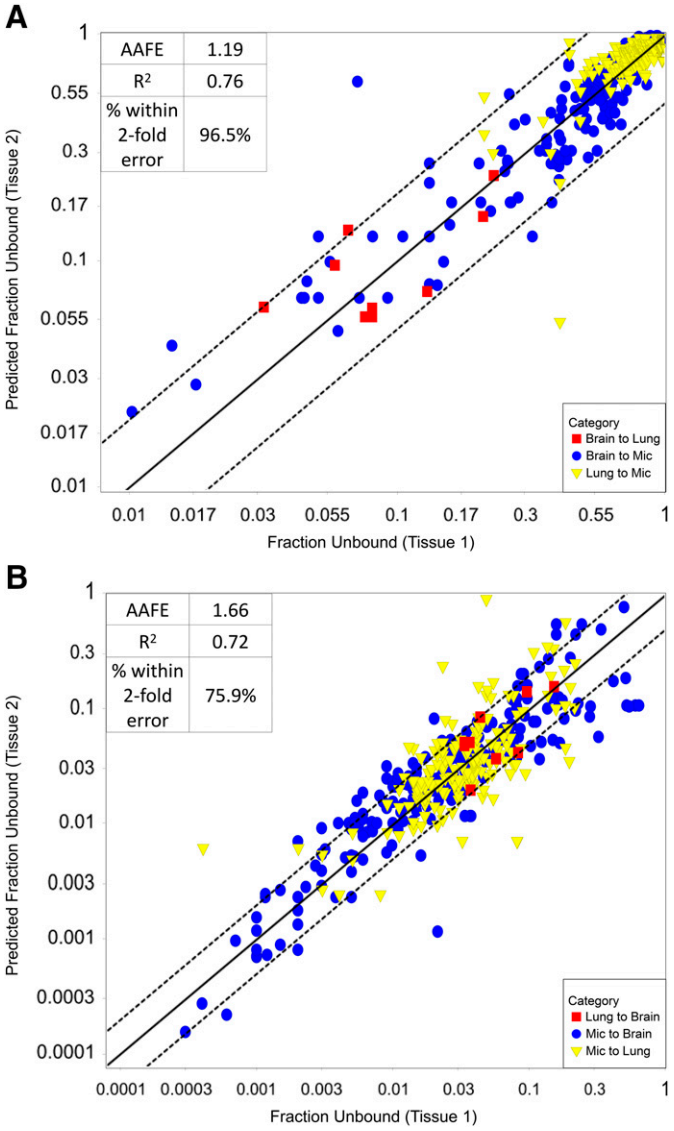

Fig. 2. Prediction of tissue binding from a tissue with higher lipid content to a tissue with lower lipid content (A) and from a tissue with lower lipid content to a tissue with higher lipid content (B). Species information is removed from the plot to support the hypothesis that tissue binding is comparable across species and tissues. $N = 399$ binding measurements. A table showing AAFE, R^2, and percentage within 2-fold error is located in the top left-hand corner of the figure. The *y*-axis and *x*-axis are presented in log scale. Solid and dotted lines represent best-fit line and 2-fold error, respectively. Dilution factors predicting fu_{mic} from fu_{brain}, fu_{mic} from fu_{lung}, and fu_{lung} from fu_{brain} were 0.0137, 0.007, and 0.59, respectively. Dilution factors predicting fu_{brain} from fu_{mic}, fu_{lung} from fu_{mic}, and fu_{brain} from fu_{lung} were 66.6, 107.8, and 1.67, respectively.

whereas Korzekwa and Nagar's fit predicted 64.1% of the V_d values within 2-fold of observed V_d. In addition, AAFE converged to a value of 1.9 for both sets of parameters. Given the high comparability in the statistics, the parameters originally derived by Korzekwa and Nagar were adopted to eliminate the bias resulting from evaluating and fitting a model on the same data set.

In rows three to seven in Table 2, Korzekwa and Nagar's fit was applied to human ($n = 60$), cyno ($n = 17$), dog ($n = 20$), mouse ($n = 110$), and rat ($n = 130$) liver microsomal data sets. The percentage within 2-fold error ranged from 62.3% to 75.0%, with rodents on the lower end of V_d prediction accuracy. AAFE values ranged from 1.61 to 1.94, but these were classified as accurate predictions since they all fell within 2.0.

TABLE 2

Methods and statistics used to evaluate Korzekwa and Nagar's model for predicting V_d

Method	Target[a]	a	b	*N*	R^2	AAFE	AFE	Within 2-fold Error	Within 3-fold Error
								%	
GNE-liver microsome	All species	18.22 ± 1.39	1.76 ± 0.28	337	0.439	1.86	1.06	65.0	86.0
KN-liver microsome[b]	All species	20 ± 0.20	0.76 ± 0.43	337	0.446	1.89	1.16	64.1	84.0
KN-liver microsome	Human	20 ± 0.20	0.76 ± 0.43	60	0.700	1.92	0.98	65.0	81.7
KN-liver microsome	Cyno	20 ± 0.20	0.76 ± 0.43	17	0.686	1.61	0.72	70.6	94.1
KN-liver microsome	Dog	20 ± 0.20	0.76 ± 0.43	20	0.342	1.72	0.89	75.0	85.0
KN-liver microsome	Mouse	20 ± 0.20	0.76 ± 0.43	110	0.332	1.89	1.22	62.7	82.7
KN-liver microsome	Rat	20 ± 0.20	0.76 ± 0.43	130	0.348	1.94	1.34	62.3	84.6
KN-brain	CDMR	20 ± 0.20	0.76 ± 0.43	105	0.517	1.79	1.34	69.5	85.7
KN-lung	CDMR	20 ± 0.20	0.76 ± 0.43	14	0.121	1.84	1.26	57.1	85.7
KN-exp fu_{mic}	CDMR	20 ± 0.20	0.76 ± 0.43	160	0.291	1.96	1.25	62.5	81.9
KN-calc fu_{mic}	CDMR	20 ± 0.20	0.76 ± 0.43	160	0.113	2.21	0.88	51.9	75.0

a, first coefficient from Korzekwa and Nagar's model; b, second coefficient from Korzekwa and Nagar's model; calc fu_{mic}, calculated fraction unbound in microsome using physiochemical properties; CDMR, cyno, dog, mouse, and rat; exp fu_{mic}, experimentally measured fraction unbound in microsome; GNE, Genentech; KN, Korzekwa and Nagar.

[a]"All species" represents human, cyno, dog, mouse, and rat.

[b]KN coefficients applied to GNE data.

A subset of the fu_{mic} data set including 160 compounds has prospective calculated fu_{mic} values available (Table 2). In this data set, the volume of distribution predictions based on experimental fu_{mic} (N = 160, AAFE = 1.96, AFE = 1.25, percentage within 2-fold error = 62.5%, percentage within 3-fold error = 81.9%) were markedly improved compared with the predictions using calculated fu_{mic} (N = 160, AAFE = 2.21, AFE = 0.88, percentage within 2-fold error = 51.9%, percentage within 3-fold error = 75.0%).

In addition to liver microsomal data sets, we used brain and lung data sets to further validate the hypothesis that tissue binding is comparable across different tissues and species, as well as to further validate Korzekwa and Nagar's model. For brain (n = 105) and lung (n = 14) data sets, the percentages of predicted V_d values within 2-fold of observed V_d values were 69.5% and 57.1%, respectively, whereas the AAFE values were 1.79 and 1.84, respectively.

To assess the applicability of Korzekwa and Nagar's model, we compared AAFE values across multiple log D ranges and ionic species; furthermore, we used allometry data to assess the accuracy of the model compared with more expensive state-of-the-art approaches (Fig. 3). Accuracy in prediction observed for compounds with a log $D_{7.4} \geq 1$ (AAFE = 1.80) was significantly higher compared with the accuracy observed for the more hydrophilic compounds (AAFE = 2.32). This result supports the hypothesis that lipophilic molecules primarily enter cells through passive mechanisms; less lipophilic molecules may enter cells through a variety of mechanisms, including passive permeation and active transport (not captured in Korzekwa and Nagar's model). Slight differences were observed when comparing AAFE values between different ionic species, with V_d predictions for acidic compounds being slightly less accurate. This could also be attributed to lower lipophilicity and higher affinity for sinusoidal uptake transporters typically observed for acidic compounds. Overall, based on the data set analyzed in this study, human V_d predictions from Korzekwa and Nagar's model (AAFE = 1.92) appear to be as accurate as rat allometry (AAFE = 1.96) and slightly less accurate than cyno (AAFE = 1.71) and dog (AAFE = 1.74) allometry. This result is not surprising since cyno and dog are anatomically closer to humans than are rodents.

Lastly, the accuracy of V_d predictions in rodents was studied as a possible predictor of the confidence in predicting V_d in higher species. When the V_d prediction in rodents is within 2-fold from the experimentally observed V_d, the same is observed in dog or cyno in 92.5% of the cases (Fig. 4). Consistently, when rodent V_d predictions are not within 2-fold from the experimentally observed V_d, only 56.0% of V_d predictions in higher preclinical species are within 2-fold from the experimentally observed V_d (Fig. 4).

Discussion

The ability of in vitro and in silico models to predict PK properties allows us to approach the in vivo experiments with quantitative hypotheses. The outcome of the in vivo experiments may either validate these hypotheses (e.g., establish an in vitro to in vivo correlation) or identify in vitro to in vivo disconnects. These findings may increase the reliance on in vitro and in vivo models, which would reduce the need for systematic preclinical PK screening, improve the quality of chemical design, and/or point to additional experiments to characterize less understood mechanisms. Findings from early mechanistic studies to investigate disconnects in in vitro to in vivo correlations may result in the early identification of a major liability for a given chemical scaffold, allowing us to refocus chemical design with a more desirable chemical space. Overall, quantitative hypotheses emerging from in vitro and

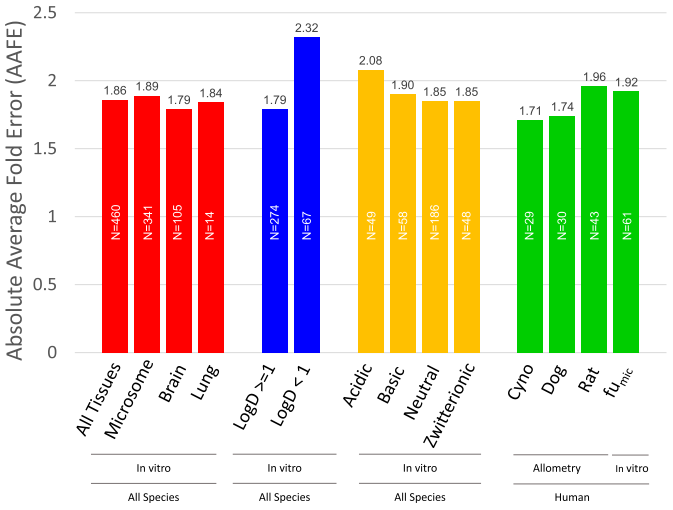

Fig. 3. Assessment of the applicability of the model based on V_d prediction accuracy for multiple tissues, log D ranges, ionic classes, and allometry. Number of compounds for each analysis is shown in each bar graph, and AAFE values are shown above each bar graph. "All species" represents human, cyno, dog, mouse, and rat.

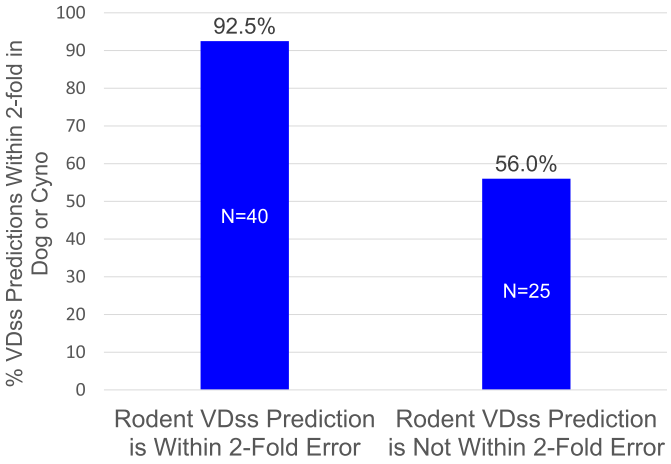

Fig. 4. Confidence in dog or cyno V_d predictions based on rodent V_d predictions. The number of compounds for each analysis is shown in each bar graph, and percentage values are shown above each bar graph. VDss, volume of distribution at steady-state.

in silico models result in saving considerable time and resources when compared with a systematic in vivo PK screening approach.

The importance of optimizing CL in the discovery process has been emphasized in many different publications and is well incorporated in the chemical design process in the form of in vitro tools, in silico tools, and design guidelines. Recently, the rational optimization of drug half-life has been emphasized in several publications, highlighting opportunities and unmet needs for reliable and practical in vitro models to be used in early research (Broccatelli et al., 2018, 2019; Gunaydin et al., 2018). Although tissue composition models significantly advanced the understanding and predictability of in vivo V_d (Oie and Tozer, 1979; Rodgers and Rowland, 2007; Poulin and Theil 2009), some of the key measurements that are required by these models are not readily available in the early phases of drug discovery (e.g., log P, pK_a). Furthermore, these models attempt to use physicochemical properties to model binding to lipids present in tissues rather than relying on a direct measurement of affinity to tissue components. Korzekwa and Nagar recognized that readily available fu_{mic} data could be used as a surrogate to estimate tissue binding; this approach is indirectly validated by Ryu et al., demonstrating that tissue binding is comparable across species and tissues. Our analysis based on a larger data set of historical measurements across several tissues (microsomes, brain, lung) essentially confirms the findings of Ryu et al. We were able to derive dilution factors allowing us to convert fu_{brain} measurements into fu_{mic} estimates with high confidence (96.5% within 2-fold error) and vice versa. However, we did see a lower prediction accuracy in the former case compared with the latter case. We also observed that the experimental error propagation in the dilution formula is asymmetric; hence, the extrapolation from a matrix with lower lipid content to a matrix with higher lipid content leads to higher error. The same phenomenon is to be expected when diluted plasma is used to estimate fu_p in plasma samples. Overall, these findings may contribute to decrease the resources needed to estimate binding in multiple tissue binding without appreciable information loss. The potential for a new paradigm exists in which in vitro tissue binding measurements in one species alone is enough to accurately predict tissue binding in other species and tissues.

The application of the model introduced by Korzekwa and Nagar to 456 compounds highlighted that brain or microsomal binding can be interchangeably used in conjunction with fu_p to predict V_d in human and preclinical species. It is particularly encouraging that refitting the two model coefficients (a and b) based on the combined external (Supplemental Table 1) and internal data set (Supplemental Table 2) of 337 compounds led to appreciable accuracy improvement over the original model proposed by Korzekwa and Nagar, which was based on a small set of human-only data. A closer analysis of the model accuracy stratified by ionic class and lipophilicity highlighted that the accuracy of the model for lipophilic compounds (log $D_{7.4} > 1$) approaches the accuracy of single-species allometry based on dog or cyno. The accuracy of the same model for compounds with log $D_{7.4} < 1$ is considerably lower, suggesting that for these chemical entities, active transporters may at times play an important role in distribution; this is in agreement with the guidelines provided by the biopharmaceutics drug distribution classification system and reinforces the expectations that the effect of drug transporters in the distribution and elimination of drugs can be expected to be important for compounds with lower lipophilicity. This simple rule of thumb may be of use when interpreting in vitro to in vivo correlations and prioritizing hypothesis-driven studies. Based on Genentech's internal data set, it was also possible to describe the model confidence in predicting V_d for dog and monkey as a function of the accuracy for V_d predictions in rodents. Not surprisingly, 92% of the V_d predictions in higher species were accurate (within 2-fold) for the compounds for which V_d predictions in rodents were also accurate. In the remaining cases, the accuracy of V_d predictions for higher species decreased to 56%. By extension, it is reasonable to expect that good in vitro to in vivo correlations in rodent will translate into high accuracy in human predictions. Although the model can use calculated fu_{mic} as an input with a reasonable degree of success, predictions using experimental fu_{mic} appear to be markedly better.

In conclusion, it is noteworthy to stress that the findings described in this paper provide new tools to approach human drug half-life optimization entirely based on readily available in vitro parameters: plasma protein binding, microsome binding, and hepatocyte stability. This could contribute to further reducing the reliance on animal experiments and accelerating the drug research and development process.

Acknowledgments

We would like to thank Ronitte Libedinsky, Matthew Wright, Christine Bowman, Yanran Wang, and Matthew Durk for reviewing and providing editing suggestions to the paper.

Authorship Contributions

Participated in research design: Hsu, Broccatelli.
Conducted experiments: Chen.
Contributed new reagents or analytic tools: Hsu, Broccatelli.
Performed data analysis: Hsu, Broccatelli.
Wrote or contributed to the writing of the manuscript: Hsu, Broccatelli.

Note Added in Proof: An incorrect 1st name for the second author was accidentally published in the Fast Forward version that appeared online February 2, 2021. The author line has now been corrected.

References

Barr JT, Lade JM, Tran TB, and Dahal UP (2019) Fraction unbound for liver microsome and hepatocyte incubations for all major species can be approximated using a single-species surrogate. *Drug Metab Dispos* **47**:419–423.

Benet LZ, Broccatelli F, and Oprea TI (2011) BDDCS applied to over 900 drugs. *AAPS J* **13**: 519–547.

Berellini G and Lombardo F (2019) An accurate in vitro prediction of human VD_{ss} based on the Øie-Tozer equation and primary physiochemical descriptors. 3. Analysis and assessment of predictivity on a large dataset. *Drug Metab Dispos* **47**:1380–1387.

Broccatelli F, Aliagas I, and Zheng H (2018) Why decreasing lipophilicity alone is often not a reliable strategy for extending IV half-life. *ACS Med Chem Lett* **9**:522–527.

Broccatelli F, E C A Hop C, and Wright M (2019) Strategies to optimize drug half-life in lead candidate identification. *Expert Opin Drug Discov* **14**:221–230.

Chen YC, Kenny JR, Wright M, Hop CECA, and Yan Z (2019) Improving confidence in the determination of free fraction for highly bound drugs using bidirectional equilibrium dialysis. *J Pharm Sci* **108**:1296–1302.
Davies B and Morris T (1993) Physiological parameters in laboratory animals and humans. *Pharm Res* **10**:1093–1095.
Gunaydin H, Altman MD, Ellis JM, Fuller P, Johnson SA, Lahue B, and Lapointe B (2018) Strategy for extending half-life in drug design and its significance. *ACS Med Chem Lett* **9**: 528–533.
Korzekwa K and Nagar S (2017) Drug distribution part 2. Predicting volume of distribution from plasma protein binding and membrane partitioning. *Pharm Res* **34**:544–551.
Leung C, Kenny JR, Hop CECA, and Yan Z (2020) Strategy for determining the free fraction of labile covalent modulators in plasma using equilibrium dialysis. *J Pharm Sci* **109**: 3181–3189.
Liang X, Ubhayakar S, Liederer BM, Dean B, Ran-Ran Qin A, Shahidi-Latham S, and Deng Y (2011) Evaluation of homogenization techniques for the preparation of mouse tissue samples to support drug discovery. *Bioanalysis* **3**:1923–1933.
Lombardo F, Berellini G, and Scott Obach R (2018) Trend analysis of a database of intravenous pharmacokinetic parameters in humans for 1352 drug compounds. *Drug Metab Dispos* **46**: 1466–1477.
Lombardo F, Waters NJ, Argikar UA, Dennehy MK, Zhan J, Gunduz M, Harriman SP, Berellini G, Rajlic IL, and Obach RS (2013) Comprehensive assessment of human pharmacokinetic prediction based on in vivo animal pharmacokinetic data, part 1: volume of distribution at steady state [published correction appears in *J Clin Pharmacol* (2013) 53:574]. *J Clin Pharmacol* **53**: 167–177.
Oie S and Tozer TN (1979) Effect of altered plasma protein binding on apparent volume of distribution. *J Pharm Sci* **68**:1203–1205.
Poulin P and Theil FP (2009) Development of a novel method for predicting human volume of distribution at steady-state of basic drugs and comparative assessment with existing methods. *J Pharm Sci* **98**:4941–4961.
Rodgers T and Rowland M (2007) Mechanistic approaches to volume of distribution predictions: understanding the processes. *Pharm Res* **24**:918–933.
Ryu S, Tess D, Chang G, Keefer C, Burchett W, Steeno GS, Novak JJ, Patel R, Atkinson K, Riccardi K, et al. (2020) Evaluation of fraction unbound across 7 tissues of 5 Species. *J Pharm Sci* **109**:1178–1190.
Waters NJ, Jones R, Williams G, and Sohal B (2008) Validation of a rapid equilibrium dialysis approach for the measurement of plasma protein binding. *J Pharm Sci* **97**:4586–4595.
Yang J, Jamei M, Yeo KR, Rostami-Hodjegan A, and Tucker GT (2007) Misuse of the well-stirred model of hepatic drug clearance. *Drug Metab Dispos* **35**:501–502.

Address correspondence to: Fabio Broccatelli, Genentech, Inc., 1 DNA Way, South San Francisco, CA 94080. E-mail: broccatf@gene.com

Article Title: Evaluation of Tissue Binding in 3 Tissues Across 5 Species, and Prediction of Volume of Distribution from Plasma Protein and Tissue Binding with an Existing Model

Authors: Frederick Hsu, Ivy Chen, Fabio Broccatelli

Journal: Drug Metabolism and Disposition

Manuscript Number: DMD-AR-2020-000337

Affiliation: Drug Metabolism & Pharmacokinetics (FH, IC, FB), Genentech, Inc., 1 DNA Way, South San Francisco, CA 94080, USA.

Table S1. Human V_d dataset for marketed drugs

Compound Name	c_pKa_MA	c_pKa_MB	fup	fumic(1mg/mL)	VDss	VDss predicted (LKL Model)	Species	a	b
Dronedarone	8.24	9.64	0.001	0.002	20	10.03	H	20	0.76
Glyburide	5.26	0.00	0.0013	0.600	0.08	0.13	H	20	0.76
Tolcapone	4.51	0.00	0.003	0.193	0.12	0.36	H	20	0.76
Mifepristone	14.00	4.51	0.0032	0.117	0.45	0.59	H	20	0.76
Nefazodone	14.00	6.87	0.0042	0.115	0.51	0.76	H	20	0.76
Rosiglitazone	6.16	5.35	0.0066	0.653	0.2	0.19	H	20	0.76
Ibuprofen	4.36	0.00	0.011	0.910	0.15	0.14	H	20	0.76
Furosemide	3.64	0	0.012	0.942	0.12	0.14	H	20	0.76
Sulfinpyrazone	2.93	0.00	0.016	0.781	0.12	0.22	H	20	0.76
Warfarin	4.94	0.00	0.023	0.685	0.13	0.35	H	20	0.76
Midazolam	14.00	5.92	0.0342	0.553	1.1	0.70	H	20	0.76
Nifedipine	14.00	3.37	0.035	0.460	0.79	0.97	H	20	0.76
Clomipramine hydrochloride	14.00	9.07	0.039	0.124	13	5.65	H	20	0.76
Chlorpromazine	14.00	9.07	0.044	0.040	10	21.53	H	20	0.76
Trazodone hydrochloride	14.00	6.87	0.053	0.818	0.52	0.41	H	20	0.76
Oxazepam	14.00	2.06	0.065	0.619	0.59	0.99	H	20	0.76
Cefoperazone	2.59	0.00	0.07	0.980	0.17	0.22	H	20	0.76
Zolpidem	14.00	4.94	0.074	0.817	0.54	0.53	H	20	0.76
Promethazine	14.00	9.03	0.096	0.242	14	6.20	H	20	0.76
Erythromycin	14.00	8.47	0.1	0.905	0.95	0.41	H	20	0.76
AmitriptylineÂ·HCl	14.00	8.83	0.12	0.250	8.7	7.43	H	20	0.76
Paroxetine	14.00	9.82	0.12	0.143	18	14.63	H	20	0.76
Imatinib	14.00	8.44	0.1251	0.523	3.9	2.51	H	20	0.76
Tolterodine	14.00	9.25	0.13	0.550	1.5	2.36	H	20	0.76
Tamsulosin	14.00	8.22	0.1461	0.887	0.21	0.63	H	20	0.76
Clonazepam	14.00	0.00	0.15	0.653	2.9	1.89	H	20	0.76
Desipramine	14.00	9.91	0.16	0.245	15	10.12	H	20	0.76
Cefazolin	2.23	0	0.18	0.980	0.12	0.41	H	20	0.76
Quinidine	14.00	9.18	0.19	0.712	2.9	1.85	H	20	0.76
Citalopram	14.00	9.77	0.2	0.706	12	1.99	H	20	0.76
Imipramine	14.00	9.07	0.2	0.365	12	7.28	H	20	0.76
Propranolol	14.00	9.18	0.21	0.925	3.1	0.68	H	20	0.76
Quinacrine	14.00	10.09	0.24	0.504	45	5.11	H	20	0.76
Verapamil	14.00	8.55	0.28	0.642	3.7	3.55	H	20	0.76
Quinine	14.00	8.19	0.3	0.792	1.8	2.03	H	20	0.76
Dexamethasone	14.00	0.00	0.32	0.665	0.94	3.73	H	20	0.76
Lidocaine	14.00	0.00	0.33	0.881	1.8	1.41	H	20	0.76
Indinavir	14.00	6.49	0.36	0.506	0.82	7.59	H	20	0.76
Diphenhydramine	14.00	8.43	0.38	0.818	6.5	2.25	H	20	0.76
Moxalactam	2.87	0	0.39	0.980	0.17	0.75	H	20	0.76
Telithromycin	14.00	8.47	0.44	1.000	3	0.64	H	20	0.76
Acetaminophen	14.00	0.00	0.52	0.959	1	1.21	H	20	0.76
Nevirapine	14.00	5.55	0.52	1.000	1.3	0.76	H	20	0.76
Tacrine	14.00	9.81	0.55	0.923	11	1.70	H	20	0.76
Almotriptan	14.00	9.09	0.6	0.887	2.2	2.38	H	20	0.76
Moxifloxacin	6.19	8.53	0.6	0.905	1.4	2.12	H	20	0.76
Atropine	14.00	9.36	0.61	0.961	3.3	1.36	H	20	0.76
Theophylline	14.00	0.00	0.61	0.965	0.51	1.32	H	20	0.76
Caffeine	14.00	0.00	0.64	1.000	0.63	0.91	H	20	0.76
Bisoprolol	14.00	9.18	0.66	0.852	2.4	3.22	H	20	0.76
Ciprofloxacin	6.13	8.61	0.7	0.835	2.1	3.75	H	20	0.76
Codeine	14.00	8.48	0.7	0.925	3.5	2.11	H	20	0.76
Venlafaxine	14.00	9.18	0.73	0.855	4.4	3.48	H	20	0.76
Zidovudine	14.00	0.00	0.8	0.825	1.8	4.51	H	20	0.76
Famotidine	14.00	6.88	0.84	1.000	1.2	1.16	H	20	0.76
Acyclovir	8.75	2.86	0.85	1.000	0.71	1.17	H	20	0.76
Metoprolol	14.00	9.18	0.88	0.898	3.1	3.21	H	20	0.76

Antipyrine	14.00	0.00	0.93	1.000	0.77	1.27	H	20	0.76
Cyclophosphamide	14.00	10.33	0.93	0.955	0.73	2.15	H	20	0.76
Atenolol	14.00	9.18	0.94	0.980	0.95	1.66	H	20	0.76

Table S2. Cynomolgus, Dog, Rat, Mouse V_d dataset for internal compounds

Compound #	Calc pKa_MA	Calc pKa_MB	fup	fubrain	fulung	fumic or Predicted fumic(1mg/mL)	VDss	VDss predicted (LKL Model)	Species	Tissue	A	B
1	14	3.4	0.48	N/A	N/A	0.9231	1.2	1.54	C	Liver Microsome	20	0.76
2	14	2.7	0.53	N/A	N/A	0.8692	1.3	2.41	C	Liver Microsome	20	0.76
3	14	2.7	0.2	N/A	N/A	0.6529	1.1	2.50	C	Liver Microsome	20	0.76
4	6.5	0	0.11	N/A	N/A	0.8182	0.59	0.75	C	Liver Microsome	20	0.76
5	14	2.7	0.21	N/A	N/A	0.8018	2	1.43	C	Liver Microsome	20	0.76
6	14	2.8	0.23	N/A	N/A	0.7241	1.7	2.17	C	Liver Microsome	20	0.76
7	14	6.3	0.12	N/A	N/A	0.4815	1.9	2.86	C	Liver Microsome	20	0.76
8	14	6.3	0.13	N/A	N/A	0.4184	1.7	3.90	C	Liver Microsome	20	0.76
9	14	6.3	0.1	N/A	N/A	0.3986	2.6	3.26	C	Liver Microsome	20	0.76
10	14	5.9	0.002	N/A	N/A	0.0438	0.43	0.99	C	Liver Microsome	20	0.76
11	14	6.7	0.08	N/A	N/A	0.7699	0.71	0.70	C	Liver Microsome	20	0.76
12	6.7	8	0.11	N/A	N/A	0.9802	0.18	0.30	C	Liver Microsome	20	0.76
13	14	6.7	0.14	N/A	N/A	0.8182	0.87	0.92	C	Liver Microsome	20	0.76
14	6.5	8	0.087	N/A	N/A	1.0000	0.27	0.23	C	Liver Microsome	20	0.76
15	14	6.7	0.19	N/A	N/A	1.0000	0.77	0.37	C	Liver Microsome	20	0.76
16	14	6.7	0.29	N/A	N/A	0.6807	0.92	3.22	C	Liver Microsome	20	0.76
17	14	6.4	0.33	N/A	N/A	0.8692	0.9	1.54	C	Liver Microsome	20	0.76
18	14	3.4	0.41	N/A	N/A	0.9231	0.99	1.29	D	Liver Microsome	20	0.76
19	14	0	0.26	N/A	N/A	0.8182	2.3	1.58	D	Liver Microsome	20	0.76
20	14	2.7	0.48	N/A	N/A	0.8692	0.78	2.14	D	Liver Microsome	20	0.76

21	14	2.7	0.22	N/A	N/A	0.6529	0.81	2.72	D	Liver Microsome	20	0.76
22	6.3	8.1	0.015	N/A	N/A	0.3889	0.44	0.60	D	Liver Microsome	20	0.76
23	6.5	0	0.13	N/A	N/A	0.8182	0.45	0.85	D	Liver Microsome	20	0.76
24	14	2.7	0.2	N/A	N/A	0.8018	1.2	1.34	D	Liver Microsome	20	0.76
25	14	2.8	0.23	N/A	N/A	0.7241	1.2	2.14	D	Liver Microsome	20	0.76
26	14	6.3	0.14	N/A	N/A	0.4815	2.2	3.30	D	Liver Microsome	20	0.76
27	14	6.3	0.072	N/A	N/A	0.4184	2.2	2.20	D	Liver Microsome	20	0.76
28	14	6.3	0.067	N/A	N/A	0.3986	2	2.21	D	Liver Microsome	20	0.76
29	14	6.7	0.15	N/A	N/A	0.7699	1.5	1.19	D	Liver Microsome	20	0.76
30	6.2	9.9	0.08	N/A	N/A	0.6949	1.4	0.91	D	Liver Microsome	20	0.76
31	6.7	8	0.17	N/A	N/A	0.9802	0.67	0.39	D	Liver Microsome	20	0.76
32	14	6.7	0.08	N/A	N/A	0.8182	0.49	0.56	D	Liver Microsome	20	0.76
33	6.5	8	0.15	N/A	N/A	1.0000	0.9	0.29	D	Liver Microsome	20	0.76
34	14	6.7	0.06	N/A	N/A	1.0000	0.44	0.18	D	Liver Microsome	20	0.76
35	14	6.7	0.14	N/A	N/A	1.0000	0.56	0.28	D	Liver Microsome	20	0.76
36	14	6.7	0.22	N/A	N/A	0.6807	0.51	2.44	D	Liver Microsome	20	0.76
37	14	6.4	0.24	N/A	N/A	0.8692	0.93	1.13	D	Liver Microsome	20	0.76
38	14	9.1	0.031	N/A	N/A	0.0753	9.4	7.74	M	Liver Microsome	20	0.76
39	8.8	8.5	0.19	N/A	N/A	0.8868	11	0.83	M	Liver Microsome	20	0.76
40	14	4.8	0.052	N/A	N/A	0.8868	0.91	0.33	M	Liver Microsome	20	0.76
41	14	3.4	0.39	N/A	N/A	0.9231	2.8	1.29	M	Liver Microsome	20	0.76
42	6.8	9.2	0.049	N/A	N/A	0.1976	5.2	4.17	M	Liver Microsome	20	0.76
43	5.2	0	0.012	N/A	N/A	0.8868	0.69	0.17	M	Liver Microsome	20	0.76

44	14	8.2	0.09	N/A	N/A	0.6393	1.8	1.22	M	Liver Microsome	20	0.76
45	14	2.7	0.61	N/A	N/A	0.8692	0.93	2.77	M	Liver Microsome	20	0.76
46	6.3	9.2	0.051	N/A	N/A	0.4286	1.8	1.55	M	Liver Microsome	20	0.76
47	14	2.7	0.25	N/A	N/A	0.6529	2.3	3.11	M	Liver Microsome	20	0.76
48	6.3	8.1	0.029	N/A	N/A	0.3889	1.1	1.07	M	Liver Microsome	20	0.76
49	14	5.3	0.014	N/A	N/A	0.1429	0.95	1.82	M	Liver Microsome	20	0.76
50	6.5	0	0.15	N/A	N/A	0.8182	2	0.99	M	Liver Microsome	20	0.76
51	6.3	4.3	0.002	N/A	N/A	0.2346	0.33	0.26	M	Liver Microsome	20	0.76
52	6.3	8.1	0.0043	N/A	N/A	0.1299	0.82	0.71	M	Liver Microsome	20	0.76
53	14	2.7	0.033	N/A	N/A	0.8018	0.76	0.33	M	Liver Microsome	20	0.76
54	14	2.8	0.21	N/A	N/A	0.7241	1.9	2.00	M	Liver Microsome	20	0.76
55	14	6.3	0.087	N/A	N/A	0.4815	1.8	2.11	M	Liver Microsome	20	0.76
56	6.7	0	0.024	N/A	N/A	0.9608	0.28	0.18	M	Liver Microsome	20	0.76
57	6.7	0	0.015	N/A	N/A	0.9048	0.3	0.18	M	Liver Microsome	20	0.76
58	14	6.3	0.032	N/A	N/A	0.4184	1.8	1.06	M	Liver Microsome	20	0.76
59	14	6.3	0.0045	N/A	N/A	0.3986	0.44	0.27	M	Liver Microsome	20	0.76
60	6.6	5.9	0.0083	N/A	N/A	0.8182	0.49	0.17	M	Liver Microsome	20	0.76
61	6.3	9.9	0.029	N/A	N/A	0.5385	1.1	0.66	M	Liver Microsome	20	0.76
62	14	5.9	0.0016	N/A	N/A	0.0438	1.1	0.82	M	Liver Microsome	20	0.76
63	14	6.7	0.078	N/A	N/A	0.7699	1.2	0.69	M	Liver Microsome	20	0.76
64	6.2	9.9	0.043	N/A	N/A	0.6949	0.32	0.56	M	Liver Microsome	20	0.76
65	5.8	8.2	0.015	N/A	N/A	0.3986	0.51	0.60	M	Liver Microsome	20	0.76
66	6.6	2.3	0.0038	N/A	N/A	0.0526	1.8	1.50	M	Liver Microsome	20	0.76

67	5.4	8.2	0.016	N/A	N/A	0.4184	0.61	0.59	M	Liver Microsome	20	0.76
68	14	6.7	0.06	N/A	N/A	0.4599	0.87	1.61	M	Liver Microsome	20	0.76
69	6.1	8.2	0.0074	N/A	N/A	0.2195	0.65	0.66	M	Liver Microsome	20	0.76
70	6.3	8.3	0.016	N/A	N/A	0.2903	0.93	0.93	M	Liver Microsome	20	0.76
71	6.6	8.1	0.0082	N/A	N/A	0.7391	0.5	0.19	M	Liver Microsome	20	0.76
72	6.6	9.9	0.022	N/A	N/A	0.6529	0.25	0.39	M	Liver Microsome	20	0.76
73	6.4	8.1	0.018	N/A	N/A	0.6529	0.21	0.34	M	Liver Microsome	20	0.76
74	6.7	9.9	0.025	N/A	N/A	0.6667	0.56	0.41	M	Liver Microsome	20	0.76
75	6.6	2.3	0.05	N/A	N/A	0.9231	1.4	0.27	M	Liver Microsome	20	0.76
76	6.7	0	0.018	N/A	N/A	0.9608	0.41	0.16	M	Liver Microsome	20	0.76
77	6.7	8	0.036	N/A	N/A	0.9802	0.72	0.19	M	Liver Microsome	20	0.76
78	14	3.8	0.013	N/A	N/A	0.1364	0.5	1.79	M	Liver Microsome	20	0.76
79	5.8	8.1	0.0073	N/A	N/A	0.2821	0.38	0.51	M	Liver Microsome	20	0.76
80	14	6.7	0.12	N/A	N/A	0.9802	0.56	0.33	M	Liver Microsome	20	0.76
81	14	9	0.21	N/A	N/A	0.8519	0.52	1.10	M	Liver Microsome	20	0.76
82	14	6.7	0.1	N/A	N/A	0.9608	0.99	0.34	M	Liver Microsome	20	0.76
83	14	9.1	0.014	N/A	N/A	0.2500	0.81	0.94	M	Liver Microsome	20	0.76
84	6.3	8.2	0.043	N/A	N/A	0.3699	0.43	1.65	M	Liver Microsome	20	0.76
85	14	9.9	0.061	N/A	N/A	0.4706	2.4	1.54	M	Liver Microsome	20	0.76
86	6.8	8.1	0.034	N/A	N/A	0.5152	0.74	0.81	M	Liver Microsome	20	0.76
87	14	9.1	0.0061	N/A	N/A	0.3605	0.58	0.31	M	Liver Microsome	20	0.76
88	4.4	2.2	0.013	N/A	N/A	0.5748	0.58	0.33	M	Liver Microsome	20	0.76
89	6.4	4.3	0.0029	N/A	N/A	0.0482	0.56	1.27	M	Liver Microsome	20	0.76

90	14	3.8	0.007	N/A	N/A	0.0929	0.7	1.50	M	Liver Microsome	20	0.76
91	14	6.8	0.81	N/A	N/A	1.0000	0.74	1.20	M	Liver Microsome	20	0.76
92	14	5.8	0.12	N/A	N/A	0.6393	0.32	1.64	M	Liver Microsome	20	0.76
93	4.8	2.3	0.92	N/A	N/A	0.9802	0.87	1.72	M	Liver Microsome	20	0.76
94	14	6.7	0.068	N/A	N/A	1.0000	0.72	0.21	M	Liver Microsome	20	0.76
95	14	4.5	0.34	N/A	N/A	0.9231	0.72	1.14	M	Liver Microsome	20	0.76
96	14	4.5	0.043	N/A	N/A	0.3423	0.54	1.83	M	Liver Microsome	20	0.76
97	8.1	10.5	0.012	N/A	N/A	0.0811	2.5	2.82	M	Liver Microsome	20	0.76
98	8.2	9.9	0.0042	N/A	N/A	0.1976	0.99	0.43	M	Liver Microsome	20	0.76
99	6.6	2.3	0.0042	N/A	N/A	0.2270	0.96	0.42	M	Liver Microsome	20	0.76
100	6.6	2.3	0.0054	N/A	N/A	0.1561	1.7	0.72	M	Liver Microsome	20	0.76
101	6.2	8.4	0.02	N/A	N/A	0.6949	0.32	0.33	M	Liver Microsome	20	0.76
102	6.3	8.8	0.046	N/A	N/A	0.5385	1	0.97	M	Liver Microsome	20	0.76
103	8	9.9	0.052	N/A	N/A	0.5873	1.3	0.89	M	Liver Microsome	20	0.76
104	6.6	2.3	0.0017	N/A	N/A	0.0267	3.4	1.37	M	Liver Microsome	20	0.76
105	3.9	3.3	0.011	N/A	N/A	1.0000	0.42	0.14	M	Liver Microsome	20	0.76
106	4	0	0.0097	N/A	N/A	0.2500	5.1	0.72	M	Liver Microsome	20	0.76
107	14	6.5	0.042	N/A	N/A	0.7391	0.67	0.48	M	Liver Microsome	20	0.76
108	14	6.5	0.031	N/A	N/A	0.9048	0.26	0.23	M	Liver Microsome	20	0.76
109	14	6.7	0.039	N/A	N/A	0.7544	2.1	0.43	M	Liver Microsome	20	0.76
110	14	6.7	0.057	N/A	N/A	0.8182	0.7	0.45	M	Liver Microsome	20	0.76
111	14	9.9	0.017	N/A	N/A	0.2422	1.7	1.17	M	Liver Microsome	20	0.76
112	14	6.7	0.087	N/A	N/A	0.8692	0.67	0.50	M	Liver Microsome	20	0.76

113	14	8.6	0.55	N/A	N/A	0.9231	2.4	1.75	M	Liver Microsome	20	0.76
114	5.8	8.7	0.011	N/A	N/A	0.1561	0.85	1.33	M	Liver Microsome	20	0.76
115	4	0	0.14	N/A	N/A	0.9608	1.1	0.42	M	Liver Microsome	20	0.76
116	6.6	2.3	0.0049	N/A	N/A	0.1765	1.9	0.59	M	Liver Microsome	20	0.76
117	14	5.8	0.034	N/A	N/A	0.1494	0.52	4.04	M	Liver Microsome	20	0.76
118	6.3	8.8	0.0077	N/A	N/A	0.1765	1.4	0.85	M	Liver Microsome	20	0.76
119	14	9.9	0.0079	N/A	N/A	0.1236	0.74	1.21	M	Liver Microsome	20	0.76
120	14	4.5	0.067	N/A	N/A	0.4925	0.76	1.59	M	Liver Microsome	20	0.76
121	6.8	8.4	0.093	N/A	N/A	0.6667	0.62	1.18	M	Liver Microsome	20	0.76
122	5.3	6	0.0096	N/A	N/A	0.0989	1.4	1.89	M	Liver Microsome	20	0.76
123	6.5	0	0.0078	N/A	N/A	1.0000	0.38	0.13	M	Liver Microsome	20	0.76
124	14	6.4	0.31	N/A	N/A	0.7699	0.79	2.39	M	Liver Microsome	20	0.76
125	8	9.9	0.22	N/A	N/A	0.6260	2.6	3.01	M	Liver Microsome	20	0.76
126	6.5	8	0.046	N/A	N/A	1.0000	0.5	0.19	M	Liver Microsome	20	0.76
127	6.5	4.2	0.39	N/A	N/A	1.0000	0.41	0.64	M	Liver Microsome	20	0.76
128	14	6.7	0.12	N/A	N/A	0.7544	0.7	1.06	M	Liver Microsome	20	0.76
129	14	9.9	0.045	N/A	N/A	0.4085	2.3	1.45	M	Liver Microsome	20	0.76
130	8.1	9.9	0.1	N/A	N/A	0.6129	1.4	1.48	M	Liver Microsome	20	0.76
131	14	6.7	0.058	N/A	N/A	0.9802	0.7	0.22	M	Liver Microsome	20	0.76
132	14	6.7	0.14	N/A	N/A	1.0000	0.51	0.31	M	Liver Microsome	20	0.76
133	4.3	3.6	0.0065	N/A	N/A	0.6393	0.32	0.21	M	Liver Microsome	20	0.76
134	14	6.7	0.14	N/A	N/A	0.9417	0.58	0.48	M	Liver Microsome	20	0.76
135	14	6.7	0.069	N/A	N/A	1.0000	0.44	0.22	M	Liver Microsome	20	0.76

136	14	6.7	0.081	N/A	N/A	0.8519	0.49	0.51	M	Liver Microsome	20	0.76
137	14	0	0.0023	N/A	N/A	0.0293	2.4	1.65	M	Liver Microsome	20	0.76
138	5.2	4.2	0.029	N/A	N/A	0.7241	0.48	0.38	M	Liver Microsome	20	0.76
139	14	6.4	0.067	N/A	N/A	1.0000	0.74	0.21	M	Liver Microsome	20	0.76
140	14	6.4	0.12	N/A	N/A	0.8692	0.6	0.64	M	Liver Microsome	20	0.76
141	14	8.2	0.062	N/A	N/A	0.1976	3	5.20	M	Liver Microsome	20	0.76
142	14	8.1	0.12	N/A	N/A	0.3333	5.2	5.05	M	Liver Microsome	20	0.76
143	4.3	3.7	0.03	N/A	N/A	0.9231	0.54	0.21	M	Liver Microsome	20	0.76
144	14	6.7	0.21	N/A	N/A	0.6807	0.56	2.37	M	Liver Microsome	20	0.76
145	4.2	3.5	0.003	N/A	N/A	0.1494	0.43	0.47	M	Liver Microsome	20	0.76
146	14	3.3	0.22	N/A	N/A	1.0000	2.9	0.42	M	Liver Microsome	20	0.76
147	14	6.4	0.12	N/A	N/A	0.8692	0.49	0.64	M	Liver Microsome	20	0.76
148	8.8	8.5	0.35	N/A	N/A	0.8868	14	1.43	R	Liver Microsome	20	0.76
149	6.8	9.2	0.05	N/A	N/A	0.1976	8.7	4.23	R	Liver Microsome	20	0.76
150	14	0	0.13	N/A	N/A	0.8182	1	0.85	R	Liver Microsome	20	0.76
151	6.3	9.2	0.022	N/A	N/A	0.4286	1.4	0.72	R	Liver Microsome	20	0.76
152	6.3	8.1	0.0035	N/A	N/A	0.3889	0.39	0.22	R	Liver Microsome	20	0.76
153	6.5	0	0.093	N/A	N/A	0.8182	1	0.64	R	Liver Microsome	20	0.76
154	5.9	0	0.0063	N/A	N/A	0.0870	0.86	1.43	R	Liver Microsome	20	0.76
155	14	3.5	0.26	N/A	N/A	0.7094	5.5	2.57	R	Liver Microsome	20	0.76
156	14	6.3	0.1	N/A	N/A	0.4815	2.2	2.39	R	Liver Microsome	20	0.76
157	6.7	0	0.021	N/A	N/A	0.9608	0.24	0.15	R	Liver Microsome	20	0.76
158	14	6.3	0.025	N/A	N/A	0.5873	1.3	0.49	R	Liver Microsome	20	0.76

159	14	6.3	0.014	N/A	N/A	0.3986	1.2	0.54	R	Liver Microsome	20	0.76
160	6.6	5.9	0.0052	N/A	N/A	0.8182	0.39	0.13	R	Liver Microsome	20	0.76
161	14	5.9	0.0095	N/A	N/A	0.0438	1.4	4.26	R	Liver Microsome	20	0.76
162	14	6.7	0.048	N/A	N/A	0.7699	0.39	0.45	R	Liver Microsome	20	0.76
163	6.2	9.9	0.015	N/A	N/A	0.6949	0.22	0.25	R	Liver Microsome	20	0.76
164	14	6.7	0.048	N/A	N/A	0.4599	2.4	1.29	R	Liver Microsome	20	0.76
165	6.3	8.3	0.0074	N/A	N/A	0.2903	0.8	0.47	R	Liver Microsome	20	0.76
166	6.7	0	0.036	N/A	N/A	0.9608	0.26	0.18	R	Liver Microsome	20	0.76
167	6.7	8	0.086	N/A	N/A	0.9802	0.29	0.25	R	Liver Microsome	20	0.76
168	14	6.3	0.13	N/A	N/A	0.6807	2.3	1.49	R	Liver Microsome	20	0.76
169	14	6.3	0.078	N/A	N/A	0.8692	2	0.44	R	Liver Microsome	20	0.76
170	14	6.7	0.025	N/A	N/A	0.4286	0.98	0.80	R	Liver Microsome	20	0.76
171	14	6.3	0.06	N/A	N/A	0.7544	1.8	0.57	R	Liver Microsome	20	0.76
172	4.4	2.2	0.0085	N/A	N/A	0.5748	1.2	0.24	R	Liver Microsome	20	0.76
173	14	6.7	0.035	N/A	N/A	0.6393	0.6	0.54	R	Liver Microsome	20	0.76
174	14	6.7	0.013	N/A	N/A	0.5625	0.53	0.32	R	Liver Microsome	20	0.76
175	14	6.7	0.05	N/A	N/A	0.6529	2.1	0.70	R	Liver Microsome	20	0.76
176	14	6.7	0.069	N/A	N/A	0.7391	2.6	0.68	R	Liver Microsome	20	0.76
177	14	6.7	0.038	N/A	N/A	0.6667	0.73	0.53	R	Liver Microsome	20	0.76
178	14	6.7	0.036	N/A	N/A	0.4925	2.3	0.89	R	Liver Microsome	20	0.76
179	14	3.9	0.092	N/A	N/A	0.7544	1.2	0.82	R	Liver Microsome	20	0.76
180	14	6.3	0.032	N/A	N/A	0.4706	2	0.86	R	Liver Microsome	20	0.76
181	14	6.7	0.037	N/A	N/A	0.5873	1.1	0.67	R	Liver Microsome	20	0.76

182	14	6.7	0.071	N/A	N/A	0.5873	1.1	1.19	R	Liver Microsome	20	0.76
183	6.5	0	0.025	N/A	N/A	1.0000	0.29	0.13	R	Liver Microsome	20	0.76
184	14	3.9	0.095	N/A	N/A	0.6529	1.3	1.24	R	Liver Microsome	20	0.76
185	14	6.3	0.074	N/A	N/A	0.7094	1.6	0.81	R	Liver Microsome	20	0.76
186	14	8.6	0.0068	N/A	N/A	0.0096	6.1	14.12	R	Liver Microsome	20	0.76
187	14	6.5	0.0041	N/A	N/A	0.9048	0.22	0.12	R	Liver Microsome	20	0.76
188	14	8	0.19	N/A	N/A	0.9048	0.91	0.72	R	Liver Microsome	20	0.76
189	14	6.7	0.071	N/A	N/A	0.8182	0.65	0.51	R	Liver Microsome	20	0.76
190	14	8.6	0.43	N/A	N/A	0.9231	4	1.36	R	Liver Microsome	20	0.76
191	5.3	9.3	0.19	N/A	N/A	0.3793	3.3	6.57	R	Liver Microsome	20	0.76
192	14	6.3	0.1	N/A	N/A	0.8018	2.3	0.73	R	Liver Microsome	20	0.76
193	5.3	8.9	0.41	N/A	N/A	0.2195	0.57	29.79	R	Liver Microsome	20	0.76
194	5	9.1	0.27	N/A	N/A	0.9608	1.3	0.67	R	Liver Microsome	20	0.76
195	5	9.1	0.22	N/A	N/A	0.7544	1.4	1.82	R	Liver Microsome	20	0.76
196	14	0	0.024	N/A	N/A	0.2121	3.5	1.92	R	Liver Microsome	20	0.76
197	14	5.8	0.021	N/A	N/A	0.1494	9.1	2.52	R	Liver Microsome	20	0.76
198	5	8	0.13	N/A	N/A	0.8182	1.1	0.85	R	Liver Microsome	20	0.76
199	5	10	0.46	N/A	N/A	1.0000	2.7	0.70	R	Liver Microsome	20	0.76
200	5	10.1	0.54	N/A	N/A	0.9231	3.1	1.71	R	Liver Microsome	20	0.76
201	14	4.5	0.037	N/A	N/A	0.4925	2.5	0.91	R	Liver Microsome	20	0.76
202	14	4.5	0.037	N/A	N/A	0.2903	6.7	1.96	R	Liver Microsome	20	0.76
203	14	6.3	0.13	N/A	N/A	0.8349	1.9	0.79	R	Liver Microsome	20	0.76
204	6.5	8	0.12	N/A	N/A	1.0000	0.89	0.26	R	Liver Microsome	20	0.76

205	14	6.7	0.16	N/A	N/A	0.7544	0.72	1.35	R	Liver Microsome	20	0.76
206	14	6.7	0.11	N/A	N/A	1.0000	0.59	0.25	R	Liver Microsome	20	0.76
207	14	4.4	0.001	N/A	N/A	0.0045	5.2	4.51	R	Liver Microsome	20	0.76
208	14	4.6	0.0045	N/A	N/A	0.0262	4.3	3.46	R	Liver Microsome	20	0.76
209	14	4.7	0.005	N/A	N/A	0.0277	3.1	3.61	R	Liver Microsome	20	0.76
210	14	6.7	0.09	N/A	N/A	1.0000	0.55	0.22	R	Liver Microsome	20	0.76
211	14	6.4	0.34	N/A	N/A	0.9802	0.89	0.68	R	Liver Microsome	20	0.76
212	14	3.8	0.24	N/A	N/A	0.8692	1.5	1.14	R	Liver Microsome	20	0.76
213	14	3.8	0.48	N/A	N/A	1.0000	1.5	0.73	R	Liver Microsome	20	0.76
214	14	0	0.0028	N/A	N/A	0.0293	4.9	1.96	R	Liver Microsome	20	0.76
215	14	0	0.0075	N/A	N/A	0.9608	1.2	0.12	R	Liver Microsome	20	0.76
216	14	3.8	0.27	N/A	N/A	0.7857	1.6	1.93	R	Liver Microsome	20	0.76
217	14	3.8	0.33	N/A	N/A	0.9802	1.8	0.67	R	Liver Microsome	20	0.76
218	14	6.4	0.096	N/A	N/A	1.0000	0.64	0.23	R	Liver Microsome	20	0.76
219	14	0	0.73	N/A	N/A	0.8349	0.87	3.94	R	Liver Microsome	20	0.76
220	14	6.2	0.29	N/A	N/A	1.0000	2.6	0.48	R	Liver Microsome	20	0.76
221	3.3	8.1	0.038	N/A	N/A	0.8692	5.6	0.27	R	Liver Microsome	20	0.76
222	14	6.4	0.16	N/A	N/A	0.8692	0.76	0.79	R	Liver Microsome	20	0.76
223	14	0	0.025	N/A	N/A	0.8519	0.62	0.22	R	Liver Microsome	20	0.76
224	14	6.7	0.38	N/A	N/A	0.7857	0.92	2.67	R	Liver Microsome	20	0.76
225	14	6.7	0.074	N/A	N/A	0.6529	0.52	0.99	R	Liver Microsome	20	0.76
226	14	6.7	0.077	N/A	N/A	0.6807	0.95	0.93	R	Liver Microsome	20	0.76
227	14	6.7	0.087	N/A	N/A	0.8868	0.72	0.44	R	Liver Microsome	20	0.76

228	14	8.2	0.047	N/A	N/A	0.3245	2.9	2.08	R	Liver Microsome	20	0.76
229	14	6.7	0.073	N/A	N/A	0.6260	0.39	1.07	R	Liver Microsome	20	0.76
230	14	6.7	0.088	N/A	N/A	0.8519	0.54	0.52	R	Liver Microsome	20	0.76
231	14	6.7	0.22	N/A	N/A	0.9608	0.49	0.57	R	Liver Microsome	20	0.76
232	14	6.7	0.12	N/A	N/A	0.8349	0.65	0.73	R	Liver Microsome	20	0.76
233	14	6.7	0.067	N/A	N/A	0.7391	0.49	0.66	R	Liver Microsome	20	0.76
234	14	6.7	0.063	N/A	N/A	0.7699	0.52	0.56	R	Liver Microsome	20	0.76
235	14	6.7	0.052	N/A	N/A	0.6129	0.45	0.83	R	Liver Microsome	20	0.76
236	14	6.7	0.19	N/A	N/A	0.6393	0.7	2.49	R	Liver Microsome	20	0.76
237	14	6.1	0.12	N/A	N/A	0.6393	2.5	1.61	R	Liver Microsome	20	0.76
238	14	8.1	0.1	N/A	N/A	0.3333	6.2	4.20	R	Liver Microsome	20	0.76
239	14	6.1	0.13	N/A	N/A	0.6667	2.6	1.57	R	Liver Microsome	20	0.76
240	14	6.4	0.41	N/A	N/A	1.0000	0.86	0.64	R	Liver Microsome	20	0.76
241	14	0	0.0023	N/A	N/A	0.0320	2.5	1.50	R	Liver Microsome	20	0.76
242	14	6.7	0.059	N/A	N/A	0.4493	0.57	1.63	R	Liver Microsome	20	0.76
243	14	6.4	0.35	N/A	N/A	1.0000	0.92	0.56	R	Liver Microsome	20	0.76
244	4.3	3.7	0.027	N/A	N/A	0.9231	1.1	0.18	R	Liver Microsome	20	0.76
245	14	0	0.77	N/A	N/A	1.0000	0.93	1.11	R	Liver Microsome	20	0.76
246	14	6.7	0.21	N/A	N/A	0.6807	0.95	2.35	R	Liver Microsome	20	0.76
247	14	6.7	0.055	N/A	N/A	0.6000	0.41	0.91	R	Liver Microsome	20	0.76
248	14	8.1	0.62	N/A	N/A	0.6667	4.8	7.10	R	Liver Microsome	20	0.76
249	14	0	0.7	N/A	N/A	1.0000	0.91	1.01	R	Liver Microsome	20	0.76
250	14	6.7	0.056	N/A	N/A	0.6529	0.38	0.77	R	Liver Microsome	20	0.76

251	14	6.4	0.23	N/A	N/A	0.9231	1	0.79	R	Liver Microsome	20	0.76
252	14	6.1	0.24	N/A	N/A	0.7857	2.9	1.72	R	Liver Microsome	20	0.76
253	14	6.4	0.052	N/A	N/A	0.8868	0.44	0.30	R	Liver Microsome	20	0.76
254	14	6.3	0.073	N/A	N/A	0.6949	0.78	0.84	R	Liver Microsome	20	0.76
255	14	6.4	0.16	N/A	N/A	0.9802	1	0.38	R	Liver Microsome	20	0.76
256	14	6.4	0.31	N/A	N/A	1.0000	1.2	0.51	R	Liver Microsome	20	0.76
257	4.2	3.5	0.0014	N/A	N/A	0.1494	0.34	0.26	R	Liver Microsome	20	0.76
258	14	8.6	0.16	N/A	N/A	0.4388	5.1	4.37	R	Liver Microsome	20	0.76
259	14	0	0.85	N/A	N/A	1.0000	0.86	1.21	R	Liver Microsome	20	0.76
260	14	0	0.69	N/A	N/A	0.9048	1.2	2.45	R	Liver Microsome	20	0.76
261	14	2.3	0.66	N/A	N/A	1.0000	1.7	0.96	R	Liver Microsome	20	0.76
262	14	6.3	0.11	N/A	N/A	0.9231	0.59	0.43	R	Liver Microsome	20	0.76
263	14	6.4	0.3	N/A	N/A	0.9608	0.97	0.74	R	Liver Microsome	20	0.76
264	14	6.4	0.1	N/A	N/A	0.8519	0.94	0.58	R	Liver Microsome	20	0.76
265	14	8.2	0.39	N/A	N/A	0.5748	7.8	6.36	R	Liver Microsome	20	0.76
266	14	0	0.77	N/A	N/A	0.9802	0.83	1.42	R	Liver Microsome	20	0.76
267	14	6.4	0.14	N/A	N/A	0.8692	0.97	0.71	R	Liver Microsome	20	0.76
268	14	6.7	0.11	N/A	N/A	0.7391	0.79	1.02	R	Liver Microsome	20	0.76
269	14	6.4	0.12	N/A	N/A	0.8018	0.92	0.85	R	Liver Microsome	20	0.76
270	14	9	0.29	N/A	N/A	0.9608	1.3	0.69	R	Liver Microsome	20	0.76
271	14	6.5	0.45	N/A	N/A	0.7857	2.6	3.14	R	Liver Microsome	20	0.76
272	14	6.7	0.18	N/A	N/A	0.9417	0.63	0.56	R	Liver Microsome	20	0.76
273	14	0	0.72	N/A	N/A	1.0000	0.93	1.04	R	Liver Microsome	20	0.76

274	14	6.4	0.36	N/A	N/A	0.9231	0.82	1.17	R	Liver Microsome	20	0.76
275	14	6.4	0.31	N/A	N/A	0.8349	1	1.73	R	Liver Microsome	20	0.76
276	8.9	6.3	0.31	N/A	N/A	1.0000	1.1	0.51	R	Liver Microsome	20	0.76
277	14	6.4	0.16	N/A	N/A	0.6949	0.54	1.72	R	Liver Microsome	20	0.76
278	14	8.8	0.1637	0.008	N/A	0.2424	16.6	10.53	C	Brain	20	0.76
279	14	8.8	0.1859	0.011	N/A	0.3062	23.8	8.75	C	Brain	20	0.76
280	14	8.8	0.2221	0.006	N/A	0.1932	19.2	18.92	C	Brain	20	0.76
281	14	8.9	0.2225	0.018	N/A	0.4211	31.7	6.49	C	Brain	20	0.76
282	14	8.4	0.191	0.068	N/A	0.7433	4.9975	1.65	C	Brain	20	0.76
283	14	5.5	0.458	0.107	N/A	0.8262	1.11	2.64	C	Brain	20	0.76
284	14	4.8	0.4432	0.133	N/A	0.8589	4.24	2.15	C	Brain	20	0.76
285	14	3.4	0.534	0.237	N/A	0.9250	1.2	1.68	C	Brain	20	0.76
286	14	2.9	0.545	0.325	N/A	0.9503	0.865	1.40	C	Brain	20	0.76
287	14	8.9	0.349	0.018	N/A	0.4211	34.3	10.11	D	Brain	20	0.76
288	14	8.8	0.3705	0.011	N/A	0.3062	25.5	17.33	D	Brain	20	0.76
289	14	8.9	0.13	0.005	N/A	0.1663	20.5	13.28	D	Brain	20	0.76
290	14	5.5	0.432	0.107	N/A	0.8262	0.684	2.45	D	Brain	20	0.76
291	14	4.8	0.6836	0.133	N/A	0.8589	2.2867	3.19	D	Brain	20	0.76
292	14	4.1	0.1642	0.019	N/A	0.4346	1.265	4.58	D	Brain	20	0.76
293	14	2.5	0.1	0.058	N/A	0.7179	2.57	1.04	M	Brain	20	0.76
294	14	8.3	0.109	0.024	N/A	0.5040	3.17	2.38	M	Brain	20	0.76
295	14	8.8	0.1307	0.011	N/A	0.3149	6.92	5.95	M	Brain	20	0.76
296	14	8.8	0.1846	0.044	N/A	0.6554	4.05	2.28	M	Brain	20	0.76
297	14	8.6	0.206	0.055	N/A	0.7063	9.52	2.08	M	Brain	20	0.76
298	14	8.4	0.132	0.068	N/A	0.7509	5.22	1.14	M	Brain	20	0.76
299	14	8.4	0.104	0.029001	N/A	0.5524	4.66	1.91	M	Brain	20	0.76
300	14	5.7	0.3341	0.24029	N/A	0.9289	2.26	1.08	M	Brain	20	0.76
301	14	9	0.3545	0.045806	N/A	0.6648	0.4322	4.14	M	Brain	20	0.76
302	14	5.8	0.282	0.124	N/A	0.8540	1.4	1.46	M	Brain	20	0.76
303	14	4.2	0.1024	0.05	N/A	0.6850	1.8	1.20	M	Brain	20	0.76
304	14	4.8	0.3837	0.133	N/A	0.8637	1.7714	1.84	M	Brain	20	0.76
305	14	2.9	0.455	0.202	N/A	0.9127	1.2103	1.60	M	Brain	20	0.76
306	14	4	0.474	0.411526	N/A	0.9666	6.1291	1.08	M	Brain	20	0.76
307	14	2.9	0.526	0.325	N/A	0.9521	1.309	1.35	M	Brain	20	0.76
308	14	0	0.702	0.6177	N/A	0.9852	0.9902	1.27	M	Brain	20	0.76
309	14	8.9	0.1008	0.018	N/A	0.4135	6.48	3.06	R	Brain	20	0.76
310	14	8.9	0.1125	0.036	N/A	0.5895	6.35	1.78	R	Brain	20	0.76
311	14	8.3	0.1357	0.024	N/A	0.4861	8.91	3.11	R	Brain	20	0.76

312	14	8.8	0.1386	0.012	N/A	0.3184	42	6.18	R	Brain	20	0.76
313	14	8.6	0.1727	0.055	N/A	0.6912	20.5	1.84	R	Brain	20	0.76
314	14	8.8	0.1788	0.044	N/A	0.6390	19.7	2.32	R	Brain	20	0.76
315	14	8.3	0.1848	0.018	N/A	0.4135	71	5.55	R	Brain	20	0.76
316	14	5.5	0.1411	0.026	N/A	0.5066	2.2	3.03	R	Brain	20	0.76
317	14	5.7	0.3652	0.24029	N/A	0.9240	2.36	1.18	R	Brain	20	0.76
318	14	5.5	0.1111	0.107	N/A	0.8217	1.79	0.73	R	Brain	20	0.76
319	14	0	0.196	0.035	N/A	0.5825	2.45	3.17	R	Brain	20	0.76
320	14	5.8	0.356	0.124	N/A	0.8448	2.725	1.87	R	Brain	20	0.76
321	14	4.1	0.5099	0.709	N/A	0.9894	1.57	0.88	R	Brain	20	0.76
322	14	4.8	0.3053	0.133	N/A	0.8551	1.7315	1.54	R	Brain	20	0.76
323	14	0	0.1031	0.04	N/A	0.6158	3.81	1.52	R	Brain	20	0.76
324	14	0	0.1131	0.252	N/A	0.9284	0.405	0.42	R	Brain	20	0.76
325	14	0	0.1162	0.057	N/A	0.6992	1.83	1.25	R	Brain	20	0.76
326	14	0	0.1172	0.076	N/A	0.7598	0.686	1.00	R	Brain	20	0.76
327	14	0	0.1213	0.09	N/A	0.7918	0.477	0.90	R	Brain	20	0.76
328	14	0	0.125	0.121	N/A	0.8411	0.86	0.74	R	Brain	20	0.76
329	14	0	0.135	0.082	N/A	0.7745	2.49	1.06	R	Brain	20	0.76
330	14	4.7	0.1634	0.06	N/A	0.7106	2.75	1.65	R	Brain	20	0.76
331	14	0	0.1649	0.117	N/A	0.8360	1.65	0.96	R	Brain	20	0.76
332	14	0	0.1821	0.067	N/A	0.7342	1.12	1.66	R	Brain	20	0.76
333	14	0	0.1904	0.128	N/A	0.8495	1.17	1.02	R	Brain	20	0.76
334	14	0	0.193	0.06309	N/A	0.7214	1.94	1.84	R	Brain	20	0.76
335	14	0	0.208	0.145	N/A	0.8671	1.51	1.01	R	Brain	20	0.76
336	14	0	0.248	0.199	N/A	0.9053	1.96	0.94	R	Brain	20	0.76
337	14	0	0.2496	0.1	N/A	0.8104	2.38	1.60	R	Brain	20	0.76
338	14	0	0.2518	0.162	N/A	0.8815	1.41	1.11	R	Brain	20	0.76
339	14	0	0.2519	0.118	N/A	0.8373	1.9	1.41	R	Brain	20	0.76
340	14	0	0.2539	0.191	N/A	0.9008	0.5247	0.99	R	Brain	20	0.76
341	14	0	0.255	0.054	N/A	0.6871	3.815	2.76	R	Brain	20	0.76
342	14	0	0.2565	0.102	N/A	0.8137	2.14	1.61	R	Brain	20	0.76
343	14	0	0.264	0.614	N/A	0.9839	0.551	0.53	R	Brain	20	0.76
344	14	0	0.2759	0.151	N/A	0.8725	0.859	1.27	R	Brain	20	0.76
345	14	0	0.2855	0.288	N/A	0.9396	1.115	0.84	R	Brain	20	0.76
346	14	0	0.2885	0.098	N/A	0.8069	2.38	1.86	R	Brain	20	0.76
347	14	0	0.2902	0.195	N/A	0.9031	0.6345	1.10	R	Brain	20	0.76
348	14	0	0.3017	0.111	N/A	0.8277	2.5	1.75	R	Brain	20	0.76
349	14	0	0.306	0.148	N/A	0.8698	0.997	1.42	R	Brain	20	0.76

350	14	0	0.3075	0.168	N/A	0.8859	2.16	1.29	R	Brain	20	0.76
351	14	0	0.3105	0.265	N/A	0.9327	1.175	0.95	R	Brain	20	0.76
352	14	0	0.3329	0.087	N/A	0.7856	3.1831	2.35	R	Brain	20	0.76
353	14	2.9	0.344	0.202	N/A	0.9069	1.65	1.26	R	Brain	20	0.76
354	14	2.6	0.3457	0.138	N/A	0.8603	1.33	1.68	R	Brain	20	0.76
355	14	0	0.3486	0.209	N/A	0.9104	1.34	1.24	R	Brain	20	0.76
356	14	0	0.3503	0.259	N/A	0.9308	1.19	1.08	R	Brain	20	0.76
357	14	0	0.3666	0.348	N/A	0.9536	1.0555	0.94	R	Brain	20	0.76
358	14	3.4	0.407	0.237	N/A	0.9228	3	1.31	R	Brain	20	0.76
359	14	0	0.412	0.306	N/A	0.9443	2.85	1.13	R	Brain	20	0.76
360	14	0	0.4438	0.241573	N/A	0.9245	1.51	1.41	R	Brain	20	0.76
361	14	0	0.4441	0.378	N/A	0.9590	1.41	1.06	R	Brain	20	0.76
362	14	0	0.468	0.324	N/A	0.9485	1.6	1.22	R	Brain	20	0.76
363	14	4.7	0.4806	0.944	N/A	0.9985	1.08	0.74	R	Brain	20	0.76
364	14	2.9	0.482	0.325	N/A	0.9488	2.055	1.25	R	Brain	20	0.76
365	14	4	0.484	0.411526	N/A	0.9642	1.09	1.09	R	Brain	20	0.76
366	14	0	0.4918	0.34	N/A	0.9520	1.32	1.24	R	Brain	20	0.76
367	14	0	0.4955	0.613	N/A	0.9839	0.896	0.91	R	Brain	20	0.76
368	14	4.7	0.5023	0.421	N/A	0.9655	1.24	1.12	R	Brain	20	0.76
369	14	0	0.5279	0.426	N/A	0.9662	0.529	1.16	R	Brain	20	0.76
370	14	0	0.5324	0.385	N/A	0.9601	0.597	1.24	R	Brain	20	0.76
371	14	2.7	0.5523	0.41	N/A	0.9639	1.87	1.24	R	Brain	20	0.76
372	14	0	0.5617	0.391	N/A	0.9611	1.29	1.29	R	Brain	20	0.76
373	14	0	0.587	0.091	N/A	0.7938	2.43	3.92	R	Brain	20	0.76
374	14	0	0.6121	0.275	N/A	0.9359	1.38	1.74	R	Brain	20	0.76
375	14	0	0.6621	0.722	N/A	0.9901	1.42	1.10	R	Brain	20	0.76
376	14	0	0.7636	0.771	N/A	0.9923	0.6655	1.22	R	Brain	20	0.76
377	14	0	0.8434	0.293	N/A	0.9410	1.15	2.26	R	Brain	20	0.76
378	14	3.1	0.1293	0.049	N/A	0.6646	3.2	1.58	R	Brain	20	0.76
379	14	2.2	0.1477	0.021	N/A	0.4521	4.09	3.88	R	Brain	20	0.76
380	14	2.5	0.2111	0.165	N/A	0.8837	1.21	0.93	R	Brain	20	0.76
381	14	2.2	0.3506	0.097	N/A	0.8051	2.47	2.26	R	Brain	20	0.76
382	14	9.5	0.2948	0.631715	N/A	0.9851	2.725	0.55	R	Brain	20	0.76
383	14	2.7	0.2045	N/A	0.075	0.8528	1.13	1.09	C	Lung	20	0.76
384	14	2.7	0.5092	N/A	0.2252	0.9540	1.27	1.27	C	Lung	20	0.76
385	14	2.7	0.2153	N/A	0.075	0.8528	0.809	1.12	D	Lung	20	0.76
386	14	2.7	0.4656	N/A	0.2252	0.9540	0.78	1.12	D	Lung	20	0.76

387	14	8.4	0.0852	N/A	0.018	0.5670	0.539	1.50	M	Lung	20	0.76
388	14	8.4	0.1237	N/A	0.028	0.6729	1.5	1.45	M	Lung	20	0.76
389	14	8.4	0.1366	N/A	0.039	0.7435	1.79	1.21	M	Lung	20	0.76
390	14	8.4	0.1579	N/A	0.041	0.7533	0.61	1.33	M	Lung	20	0.76
391	14	2.7	0.2019	N/A	0.075	0.8528	2.29	1.09	M	Lung	20	0.76
392	14	2.7	0.4255	N/A	0.2252	0.9540	0.934	1.10	M	Lung	20	0.76
393	14	2.7	0.1848	N/A	0.075	0.8528	2.12	0.98	R	Lung	20	0.76
394	14	8.4	0.2153	N/A	0.041	0.7533	5.99	1.76	R	Lung	20	0.76
395	8.8	8.5	0.2654	N/A	0.0634	0.8286	14	1.52	R	Lung	20	0.76
396	14	2.7	0.3946	N/A	0.2252	0.9540	1.62	1.00	R	Lung	20	0.76

Table S3. Calculated fu_{mic} from physiochemical properties for V_d predictions

Compound Name	c_pKa_ MA	c_pKa_ MB	fup	Expfumic (1mg/mL)	Calcfumic (1mg/mL)	VDss	VDss predicted (expfumic)	VDss predicted (calcfumic)	Species	a	b
1	14	6.7	0.14	0.8182	0.6129	0.87	0.92	2.07	C	20	0.76
2	14	6.7	0.19	1.0000	0.6807	0.77	0.37	2.15	C	20	0.76
3	14	6.4	0.33	0.8692	0.7241	0.9	1.54	3.06	C	20	0.76
4	14	6.7	0.29	0.6807	0.7699	0.92	3.22	2.23	C	20	0.76
5	6.5	8	0.087	1.0000	0.8692	0.27	0.23	0.49	C	20	0.76
6	14	3.4	0.48	0.9231	0.9048	1.2	1.54	1.75	C	20	0.76
7	14	6.7	0.08	0.8182	0.6129	0.49	0.56	1.22	D	20	0.76
8	14	6.7	0.14	1.0000	0.6807	0.56	0.28	1.59	D	20	0.76
9	14	6.7	0.06	1.0000	0.7094	0.44	0.18	0.68	D	20	0.76
10	14	6.4	0.24	0.8692	0.7241	0.93	1.13	2.23	D	20	0.76
11	14	6.7	0.22	0.6807	0.7699	0.51	2.44	1.69	D	20	0.76
12	6.5	8	0.15	1.0000	0.8692	0.9	0.29	0.74	D	20	0.76
13	14	3.4	0.41	0.9231	0.9048	0.99	1.29	1.47	D	20	0.76
14	14	5.3	0.014	0.1429	0.0417	0.95	1.82	6.58	M	20	0.76
15	6.6	2.3	0.0017	0.0267	0.0526	3.4	1.37	0.74	M	20	0.76
16	14	9.9	0.045	0.4085	0.0989	2.3	1.45	8.34	M	20	0.76
17	4.2	3.5	0.003	0.1494	0.1561	0.43	0.47	0.45	M	20	0.76
18	14	9.9	0.0079	0.1236	0.1628	0.74	1.21	0.91	M	20	0.76
19	6.6	2.3	0.0054	0.1561	0.2195	1.7	0.72	0.52	M	20	0.76
20	4	0	0.0097	0.2500	0.2270	5.1	0.72	0.80	M	20	0.76
21	6.6	2.3	0.0049	0.1765	0.2500	1.9	0.59	0.42	M	20	0.76
22	6.3	4.3	0.002	0.2346	0.2579	0.33	0.26	0.24	M	20	0.76
23	14	6.4	0.31	0.7699	0.2821	0.79	2.39	16.32	M	20	0.76
24	8.1	9.9	0.1	0.6129	0.2903	1.4	1.48	5.11	M	20	0.76
25	6.3	8.8	0.0077	0.1765	0.3072	1.4	0.85	0.48	M	20	0.76
26	8	9.9	0.22	0.6260	0.3333	2.6	3.01	9.18	M	20	0.76
27	14	9.9	0.017	0.2422	0.3514	1.7	1.17	0.73	M	20	0.76
28	5.3	6	0.0096	0.0989	0.3605	1.4	1.89	0.48	M	20	0.76
29	14	5.8	0.034	0.1494	0.3605	0.52	4.04	1.38	M	20	0.76
30	5.8	8.7	0.011	0.1561	0.3889	0.85	1.33	0.48	M	20	0.76
31	6.2	8.4	0.02	0.6949	0.4085	0.32	0.33	0.73	M	20	0.76
32	4.3	3.7	0.03	0.9231	0.4493	0.54	0.21	0.90	M	20	0.76
33	6.8	8.4	0.093	0.6667	0.4493	0.62	1.18	2.53	M	20	0.76
34	8	9.9	0.052	0.5873	0.4599	1.3	0.89	1.38	M	20	0.76
35	14	9.1	0.031	0.0753	0.4706	9.4	7.74	0.82	M	20	0.76
36	14	6.4	0.067	1.0000	0.4925	0.74	0.21	1.59	M	20	0.76
37	14	6.7	0.039	0.7544	0.5038	2.1	0.43	0.94	M	20	0.76
38	3.9	3.3	0.011	1.0000	0.5504	0.42	0.14	0.32	M	20	0.76
39	14	6.5	0.031	0.9048	0.5748	0.26	0.23	0.62	M	20	0.76
40	14	6.5	0.042	0.7391	0.5748	0.67	0.48	0.80	M	20	0.76
41	14	6.7	0.058	0.9802	0.6000	0.7	0.22	0.97	M	20	0.76
42	14	6.7	0.057	0.8182	0.6129	0.7	0.45	0.92	M	20	0.76
43	6.5	0	0.0078	1.0000	0.6260	0.38	0.13	0.23	M	20	0.76
44	6.3	8.8	0.046	0.5385	0.6260	1	0.97	0.73	M	20	0.76
45	14	4.5	0.067	0.4925	0.6260	0.76	1.59	1.01	M	20	0.76
46	14	6.7	0.12	0.7544	0.6260	0.7	1.06	1.72	M	20	0.76
47	14	8.6	0.55	0.9231	0.6529	2.4	1.75	6.68	M	20	0.76
48	8.8	8.5	0.19	0.8868	0.6667	11	0.83	2.24	M	20	0.76
49	14	6.7	0.069	1.0000	0.6807	0.44	0.22	0.86	M	20	0.76
50	14	6.7	0.14	1.0000	0.7094	0.51	0.31	1.46	M	20	0.76
51	4.3	3.6	0.0065	0.6393	0.7241	0.32	0.21	0.18	M	20	0.76
52	14	6.4	0.12	0.8692	0.7241	0.49	0.64	1.20	M	20	0.76
53	14	6.4	0.12	0.8692	0.7241	0.6	0.64	1.20	M	20	0.76
54	14	6.7	0.21	0.6807	0.7699	0.56	2.37	1.66	M	20	0.76
55	14	6.7	0.081	0.8519	0.7857	0.49	0.51	0.67	M	20	0.76
56	5.2	4.2	0.029	0.7241	0.8018	0.48	0.38	0.31	M	20	0.76
57	14	8.2	0.062	0.1976	0.8018	3	5.20	0.47	M	20	0.76
58	4	0	0.14	0.9608	0.8018	1.1	0.42	1.00	M	20	0.76
59	14	3.3	0.22	1.0000	0.8018	2.9	0.42	1.50	M	20	0.76
60	14	6.7	0.087	0.8692	0.8349	0.67	0.50	0.58	M	20	0.76

61	14	8.1	0.12	0.3333	0.8349	5.2	5.05	0.72	M	20	0.76
62	14	6.7	0.14	0.9417	0.8519	0.58	0.48	0.80	M	20	0.76
63	6.5	8	0.046	1.0000	0.8692	0.5	0.19	0.32	M	20	0.76
64	6.6	2.3	0.05	0.9231	0.8692	1.4	0.27	0.34	M	20	0.76
65	14	3.4	0.39	0.9231	0.9048	2.8	1.29	1.46	M	20	0.76
66	6.5	4.2	0.39	1.0000	0.9417	0.41	0.64	1.12	M	20	0.76
67	14	0	0.0023	0.0320	0.0050	2.5	1.50	9.21	R	20	0.76
68	14	8.6	0.0068	0.0096	0.0050	6.1	14.12	27.00	R	20	0.76
69	14	4.4	0.001	0.0045	0.0582	5.2	4.51	0.43	R	20	0.76
70	14	4.7	0.005	0.0277	0.0811	3.1	3.61	1.24	R	20	0.76
71	14	4.6	0.0045	0.0262	0.0929	4.3	3.46	0.99	R	20	0.76
72	4.2	3.5	0.0014	0.1494	0.1561	0.34	0.26	0.26	R	20	0.76
73	14	4.5	0.037	0.2903	0.1976	6.7	1.96	3.16	R	20	0.76
74	14	0	0.024	0.2121	0.2422	3.5	1.92	1.64	R	20	0.76
75	8.9	6.3	0.31	1.0000	0.3245	1.1	0.51	13.41	R	20	0.76
76	14	5.8	0.021	0.1494	0.3605	9.1	2.52	0.87	R	20	0.76
77	14	8.6	0.16	0.4388	0.3986	5.1	4.37	5.11	R	20	0.76
78	14	0	0.0075	0.9608	0.4184	1.2	0.12	0.32	R	20	0.76
79	4.3	3.7	0.027	0.9231	0.4493	1.1	0.18	0.80	R	20	0.76
80	14	6.3	0.074	0.7094	0.4706	1.6	0.81	1.86	R	20	0.76
81	14	3.9	0.095	0.6529	0.4925	1.3	1.24	2.18	R	20	0.76
82	14	6.4	0.096	1.0000	0.4925	0.64	0.23	2.21	R	20	0.76
83	14	6.3	0.1	0.8018	0.4925	2.3	0.73	2.29	R	20	0.76
84	14	6.4	0.16	0.9802	0.4925	1	0.38	3.61	R	20	0.76
85	14	8.2	0.047	0.3245	0.5267	2.9	2.08	0.97	R	20	0.76
86	14	6.3	0.073	0.6949	0.5267	0.78	0.84	1.51	R	20	0.76
87	14	6.1	0.12	0.6393	0.5504	2.5	1.61	2.22	R	20	0.76
88	14	6.5	0.0041	0.9048	0.5748	0.22	0.12	0.17	R	20	0.76
89	14	6.3	0.11	0.9231	0.6000	0.59	0.43	1.71	R	20	0.76
90	14	6.1	0.24	0.7857	0.6000	2.9	1.72	3.62	R	20	0.76
91	14	6.7	0.071	0.8182	0.6129	0.65	0.51	1.09	R	20	0.76
92	5	10.1	0.54	0.9231	0.6129	3.1	1.71	7.63	R	20	0.76
93	14	4.5	0.037	0.4925	0.6260	2.5	0.91	0.59	R	20	0.76
94	14	6.7	0.16	0.7544	0.6260	0.72	1.35	2.22	R	20	0.76
95	14	6.4	0.31	1.0000	0.6260	1.2	0.51	4.21	R	20	0.76
96	14	6.7	0.11	0.7391	0.6393	0.79	1.02	1.49	R	20	0.76
97	14	6.7	0.077	0.6807	0.6529	0.95	0.93	1.02	R	20	0.76
98	14	6.3	0.13	0.8349	0.6529	1.9	0.79	1.65	R	20	0.76
99	14	6.4	0.35	1.0000	0.6529	0.92	0.56	4.28	R	20	0.76
100	14	8.6	0.43	0.9231	0.6529	4	1.36	5.21	R	20	0.76
101	14	6.7	0.055	0.6000	0.6667	0.41	0.91	0.72	R	20	0.76
102	14	6.7	0.059	0.4493	0.6667	0.57	1.63	0.77	R	20	0.76
103	14	6.4	0.1	0.8519	0.6667	0.94	0.58	1.23	R	20	0.76
104	14	6.1	0.13	0.6667	0.6667	2.6	1.57	1.57	R	20	0.76
105	5	9.1	0.22	0.7544	0.6667	1.4	1.82	2.59	R	20	0.76
106	8.8	8.5	0.35	0.8868	0.6667	14	1.43	4.03	R	20	0.76
107	14	6.7	0.09	1.0000	0.6807	0.55	0.22	1.06	R	20	0.76
108	5	10	0.46	1.0000	0.6807	2.7	0.70	5.02	R	20	0.76
109	14	0	0.025	0.8519	0.7094	0.62	0.22	0.34	R	20	0.76
110	14	6.7	0.11	1.0000	0.7094	0.59	0.25	1.15	R	20	0.76
111	14	6.4	0.14	0.8692	0.7241	0.97	0.71	1.35	R	20	0.76
112	14	6.4	0.16	0.8692	0.7241	0.76	0.79	1.53	R	20	0.76
113	5.3	8.9	0.41	0.2195	0.7391	0.57	29.79	3.53	R	20	0.76
114	14	6.7	0.074	0.6529	0.7544	0.52	0.99	0.68	R	20	0.76
115	5	8	0.13	0.8182	0.7544	1.1	0.85	1.12	R	20	0.76
116	5.3	9.3	0.19	0.3793	0.7544	3.3	6.57	1.59	R	20	0.76
117	5	9.1	0.27	0.9608	0.7544	1.3	0.67	2.21	R	20	0.76
118	14	6.4	0.3	0.9608	0.7544	0.97	0.74	2.45	R	20	0.76
119	14	6.7	0.052	0.6129	0.7699	0.45	0.83	0.48	R	20	0.76
120	14	6.7	0.063	0.7699	0.7699	0.52	0.56	0.56	R	20	0.76
121	14	6.7	0.19	0.6393	0.7699	0.7	2.49	1.49	R	20	0.76
122	14	6.7	0.21	0.6807	0.7699	0.95	2.35	1.63	R	20	0.76
123	14	6.4	0.34	0.9802	0.7699	0.89	0.68	2.58	R	20	0.76
124	14	6.7	0.056	0.6529	0.7857	0.38	0.77	0.48	R	20	0.76
125	14	6.4	0.052	0.8868	0.8018	0.44	0.30	0.43	R	20	0.76
126	14	6.7	0.067	0.7391	0.8018	0.49	0.66	0.52	R	20	0.76

127	14	6.4	0.23	0.9231	0.8018	1	0.79	1.54	R	20	0.76
128	14	3.8	0.24	0.8692	0.8018	1.5	1.14	1.60	R	20	0.76
129	14	6.7	0.087	0.8868	0.8182	0.72	0.44	0.60	R	20	0.76
130	14	6.7	0.12	0.8349	0.8182	0.65	0.73	0.79	R	20	0.76
131	14	3.8	0.33	0.9802	0.8182	1.8	0.67	2.00	R	20	0.76
132	14	0	0.73	0.8349	0.8182	0.87	3.94	4.30	R	20	0.76
133	14	8.1	0.1	0.3333	0.8349	6.2	4.20	0.59	R	20	0.76
134	14	6.4	0.31	0.8349	0.8349	1	1.73	1.73	R	20	0.76
135	14	6.4	0.36	0.9231	0.8349	0.82	1.17	2.00	R	20	0.76
136	14	6.7	0.38	0.7857	0.8349	0.92	2.67	2.10	R	20	0.76
137	14	6.4	0.41	1.0000	0.8349	0.86	0.64	2.26	R	20	0.76
138	14	6.4	0.12	0.8018	0.8519	0.92	0.85	0.68	R	20	0.76
139	14	9	0.29	0.9608	0.8519	1.3	0.69	1.46	R	20	0.76
140	14	6.2	0.29	1.0000	0.8519	2.6	0.48	1.49	R	20	0.76
141	14	6.7	0.073	0.6260	0.8692	0.39	1.07	0.42	R	20	0.76
142	14	6.7	0.088	0.8519	0.8692	0.54	0.52	0.48	R	20	0.76
143	6.5	8	0.12	1.0000	0.8692	0.89	0.26	0.62	R	20	0.76
144	14	6.7	0.18	0.9417	0.8692	0.63	0.56	0.88	R	20	0.76
145	14	0	0.72	1.0000	0.8692	0.93	1.04	3.21	R	20	0.76
146	14	8	0.19	0.9048	0.8868	0.91	0.72	0.80	R	20	0.76
147	14	3.8	0.27	0.7857	0.8868	1.6	1.93	1.14	R	20	0.76
148	14	3.8	0.48	1.0000	0.8868	1.5	0.73	1.95	R	20	0.76
149	14	0	0.77	0.9802	0.8868	0.83	1.42	3.07	R	20	0.76
150	3.3	8.1	0.038	0.8692	0.9048	5.6	0.27	0.23	R	20	0.76
151	14	0	0.85	1.0000	0.9231	0.86	1.21	2.63	R	20	0.76
152	14	6.4	0.16	0.6949	0.9417	0.54	1.72	0.51	R	20	0.76
153	14	6.7	0.22	0.9608	0.9417	0.49	0.57	0.66	R	20	0.76
154	14	8.2	0.39	0.5748	0.9417	7.8	6.36	1.07	R	20	0.76
155	14	6.5	0.45	0.7857	0.9417	2.6	3.14	1.25	R	20	0.76
156	14	2.3	0.66	1.0000	0.9417	1.7	0.96	1.78	R	20	0.76
157	14	0	0.69	0.9048	0.9417	1.2	2.45	1.85	R	20	0.76
158	14	0	0.7	1.0000	0.9417	0.91	1.01	1.88	R	20	0.76
159	14	0	0.77	1.0000	0.9417	0.93	1.11	2.06	R	20	0.76
160	14	8.1	0.62	0.6667	1.0000	4.8	7.10	0.90	R	20	0.76